Jumbo phage-mediated transduction of genomic islands

Yansong Zhao[1,*], Yue Ma[2], Christina Vasileiou[1], Andrew D. Farr[1], David W. Rogers[1] & Paul B. Rainey[1,3,*]

[1] Department of Microbial Population Biology, Max Planck Institute for Evolutionary Biology, Plön, Germany

[2] Guest Group Evolutionary Medicine, Max Planck Institute for Evolutionary Biology, Plön, Germany

[3] Laboratory of Biophysics and Evolution, CBI, ESPCI Paris, Université PSL, CNRS, Paris, France

* To whom correspondence may be addressed. Emails: Y.Z. (yansongzhao@evolbio.mpg.de), P.B.R. (rainey@evolbio.mpg.de).

Abstract

Bacteria acquire new genes by horizontal gene transfer (HGT), typically mediated by mobile genetic elements (MGEs). While plasmids, bacteriophages and certain integrative and conjugative elements (ICEs) are well characterized, the broader diversity of MGEs remains poorly understood. Here, we propagated the bacterium *Pseudomonas fluorescens* SBW25 in the presence of filtrate obtained from garden compost communities. Genome sequencing of derived colonies revealed acquisition of three different mobile elements, each integrated immediately downstream of *tmRNA*, flanked by direct repeats, and encoding a tyrosine integrase (*intY*) and putative phage defense systems. Absent are genes with recognized roles in autonomous transfer. Interrogation of DNA sequence databases showed that similar elements are widespread in the genus *Pseudomonas* and beyond, with *Vibrio* Pathogenicity Island-1 (VPI-1) from *V. cholerae* as a notable example. Bioinformatic analyses demonstrate frequent horizontal transfer among diverse hosts. Detailed analysis of a single element, I55, showed that it is transferred between cells by a jumbo phage, and confers a fitness benefit via a type II restriction-modification system.

Significance Statement

The impact of horizontal gene transfer on the evolution of bacteria outpaces that driven by spontaneous mutation, but knowledge of the range of mediators, the genes mobilized, and the mechanisms of movement have largely depended on inferences stemming from bioinformatics. Here we describe a real-time evolution experiment in which a single focal strain propagated with filtrate from a complex microbial community captured genetic elements carrying a diverse cargo of genes whose mobility was previously uncharacterized. The elements represent a widespread class of mobile DNA dependent only on a tyrosine integrase targeting a highly conserved genomic site. Genetic analysis of one element shows that it confers a significant fitness advantage via defense against bacteriophages, and hijacks a jumbo bacteriophage for intercellular transfer. Our findings reveal new insights into the hidden diversity and dynamics of MGEs in natural environments.

Classification

Biological Sciences / Microbiology

Key Words

experimental evolution – comparative genomics – phage satellites – jumbo bacteriophages

Introduction

Mobile genetic elements (MGEs), such as bacteriophages, plasmids, and integrative and conjugative elements (ICEs), play a central role in shaping the structure and function of microbial communities (Arnold et al., 2022). In addition to driving their own replicative capacity, MGEs often capture and disseminate ecologically significant genes among bacterial hosts, facilitating horizontal gene transfer (HGT) (Arnold et al., 2022; Dmitrijeva et al., 2024; Quistad et al., 2020). Recent theoretical and experimental work suggests that accessory genes disseminated by MGEs may act as "community genes," promoting feedbacks that underpin differential persistence and enabling selection to operate at the level of communities (Doolittle, 2024; Doolittle & Inkpen, 2018; Lenton et al., 2021; Rainey & Quistad, 2020; Roughgarden, 2020).

While classical genetics has led to discovery of various mechanisms of HGT, including conjugation (Lederberg & Tatum, 1946), transduction (Zinder & Lederberg, 1952) and transformation (Griffith, 1928), the majority of recent discoveries stem from genome analyses (Dmitrijeva et al., 2024; Groussin et al., 2021; Hackl et al., 2023). Comparisons among closely related strains frequently reveal regions with contrasting evolutionary histories, often termed "genomic islands" (GIs), which are inferred to have arisen via HGT (Koutsovoulos et al., 2022; Yuan et al., 2023). While instructive, such bioinformatic methods rarely provide insight into the causes of horizontal movement. Notable exceptions include demonstration of the mobility of ICEs (Colombi et al., 2017; J. T. Sullivan & Ronson, 1998), of plasmids (Hall et al., 2016; Lilley & Bailey, 1997b), of gene transfer agents (Lang et al., 2012; Marrs, 1974), and of phage-inducible chromosomal islands (PICIs) (Barcia-Cruz et al., 2024; Fillol-Salom et al., 2019; Lindsay et al., 1998; Novick et al., 2010). PICIs, a class of phage satellite (Ibarra-Chávez et al., 2021; Penadés et al., 2025), hitchhike with, or hijack, bacteriophages to facilitate their own intercellular transfer.

Experimental evolution, where populations or communities are propagated under controlled conditions (Lenski, 2017; Rainey et al., 2017; Rainey & Travisano, 1998), offers a powerful means to explore evolutionary processes. Although rarely used to study HGT directly, experimental evolution provides opportunities to track the dissemination of genes, identify the mediators of transfer, and uncover functional consequences (Frazão et al., 2019; Hall et al., 2016; Lilley & Bailey, 1997a; Quistad et al., 2020; Woods et al., 2020). For example, Quistad et al. (Quistad et al., 2020), used experimental evolution of compost-derived microbial communities to show that manipulation of MGE activity influenced the flux of horizontally disseminated DNA (van Dijk et al., 2023), but in the absence of culturable hosts carrying newly acquired DNA – underpinned by further analyses of fitness and genetics – understanding is limited to inferences stemming from bioinformatics.

In this study, we use experimental evolution to detect, isolate and characterize MGEs from environmental sources. Building on the approach of Quistad et al. (Quistad et al., 2020) we simplified the system by propagating a single bacterium, *Pseudomonas fluorescens* SBW25 (Fortmann-Grote et al., 2023; Silby et al., 2009), in the presence of filtrate derived from complex compost communities. This led to capture of three GIs lacking any evidence of autonomous capacity for horizontal transfer. Each element integrates immediately downstream of *tmRNA*, varies in size and gene content, and encodes putative phage defense systems. Bioinformatic analyses based on a minimal set of core genes revealed these elements to be widespread across *Pseudomonas* and beyond, with frequent signatures of horizontal transfer. Detailed analysis of a single element, I55, showed that it is transferred between cells

85 by a jumbo phage present in the compost filtrate, and confers a fitness benefit via a type II restriction-
86 modification system.

Results

Pseudomonas fluorescens SBW25 propagated in the presence of compost filtrate acquires mobile genetic elements

To investigate whether *P. fluorescens* SBW25 could acquire MGEs from environmental sources, we used a simple mark-recapture approach (Fig. 1a(ii)). Initially, SBW25 was marked with gentamicin resistance (strain MPB28806) and propagated under static conditions in microcosms containing a wash from compost communities. Unfortunately, SBW25 rapidly went extinct (Fig. E1). To reduce competition and risk of competitive exclusion, we propagated SBW25 carrying kanamycin resistance and either GFP or RFP markers (strains MPB29284 and MPB29300, respectively) in the presence of filtrate from compost communities, employing two regimes: a "live-filtrate" regime and a "fixed-filtrate" regime (Fig. 1a(i) and 1a(iii), respectively). In both cases, filtrate was prepared by passing community cultures through 0.2 µm filters to remove cells while retaining phage-sized particles and other small entities (Quistad et al., 2020).

In the live-filtrate regime, material was freshly obtained from a compost community (compost C) synchronized with the evolution experiment, with 50 µL filtrate added to each of eight replicate SBW25 populations at every transfer over 14 serial passages. In the fixed-filtrate regime, filtrate was prepared once from independent compost communities (composts B, C, and D), stored at −80 °C, and added to 10 replicate populations per compost source for seven serial transfers. Following the final transfer, colonies were isolated from each replicate for whole-genome sequencing: two to three colonies per replicate in the live-filtrate regime, and pools of 24 colonies per replicate in the fixed-filtrate regime.

Mapping colony (or pooled-colony) sequencing reads back to the SBW25 reference genome revealed the acquisition of foreign DNA sequences (Fig. 1b). Further analysis identified three distinct GIs, designated I23, I44, and I55 (approximately 23 kb, 44 kb, and 55 kb in size, respectively), recovered on five independent occasions (Fig. 1c). From the 19 colonies sequenced from the live-filtrate regime, one contained I55 (strain MPB33357), which was acquired from compost C. Of the 720 colonies sequenced from the fixed-filtrate regime, six contained I23 (strains MPB38392, MPB38393, MPB38394, MPB38395, MPB38396, MPB38895) and two contained I44 (strains MPB38906, MPB38907). I23 was acquired independently on three occasions from compost B; I44 was detected in just a single replicate receiving filtrate from compost B.

Mapping the ends of contigs containing each element confirmed that all three GIs inserted at the same genomic locus, immediately downstream of *tmRNA* and immediately upstream of a putative mobilizable genomic island PFI-12 (see Fig. 1d). This was confirmed by PCR analysis. Each element is flanked by a 14 bp direct repeat (CCC CGG CTC CAC CA), corresponding to the second half of the *attP* site described in *Pseudomonas aeruginosa* PAO1 (Fiedoruk et al., 2020). One copy of the 14 bp sequence is located in the SBW25 genome, spanning the final 11 bp of *tmRNA* and 3 bp immediately downstream, while the second copy is introduced upon integration of the mobile element.

Each element harbors a gene encoding a tyrosine integrase (IntY, I23-*orf01*, I44-*orf01*, I55-*orf01*) near the 5'-end and a gene encoding AlpA (I23-*orf20*, I44-*orf32*, I55-*orf39*), a putative transcriptional activator of *intY* (Barcia-Cruz et al., 2024; X. Wang et al., 2009), at the 3'-end (see Fig. 1e). It is likely that IntY catalyzes site-specific recombination of the MGE into the genome, with the 14 bp direct repeat being the common core sequence (Grindley et al., 2006; Groth & Calos, 2004). The integrases each show

128 ~20% divergence at the nucleotide level; *alpA* in I44 and I55 are identical, but ~20% dissimilar to *alpA*
129 from I23. Recombination thus impacts evolution of the elements.

130 Beyond the shared integration site and presence of *intY* plus *alpA*, the three elements share a ~18 kb
131 region of sequence similarity at the 3'-end, although I44 and I55 contain gaps (see Fig. 1e for alignment,
132 and Table S4 for detailed annotations). The region encodes YqaJ (I23-*orf06*, I44-*orf23*, I55-*orf28*), an
133 HTH-containing protein (I23-*orf11*, I44-*orf28*, I55-*orf32*), an inovirus Gp2-like protein (I23-*orf19*, I44-
134 *orf31*, I55-*orf38*), along with many open reading frames predicted to encode proteins with no matches
135 to either DNA or protein sequence databases. Some elements, notably I23 and I55, also encode a
136 putative DNA methyltransferase predicted to function as a type II restriction-modification system (Tock
137 & Dryden, 2005).

138 Between *intY* and the region of similarity – and accounting for length differences – are various cargo
139 genes that differ among the three MGEs. However, all three elements encode genes predicted by
140 DefenseFinder (Tesson et al., 2022) to confer protection against phages (Fig. 1e). I23 encodes a Gabija
141 system (*orf02-orf03*) (Cheng et al., 2023; Doron et al., 2018); I55 encodes dynamins (*orf02-orf03*) and
142 RecBCD (*orf23-orf25*) ; I44 encodes a classic type II restriction-modification system (*orf02-orf03*) (Tock &
143 Dryden, 2005) and a DISARM system (*orf05-orf10*) (Ofir et al., 2017). In addition, I44 encodes a ~14 kb
144 operon (*orf11-orf20*) composed of metabolic genes including putative hydantoinases (Ishikawa et al.,
145 1997), a peptidase M24, and an Asp/Glu/hydantoin racemase.

146 Given that the three elements were acquired during the course of serial transfer experiments, they must
147 be capable of either autonomous, or non-autonomous transfer. A search of encoded genes showed no
148 evidence of those associated with lateral transmission, such as bacterial insertion sequences (Xie &
149 Tang, 2017), typical virus or plasmid structures (Camargo et al., 2023; de Sousa et al., 2023), or
150 machinery for conjugation (Néron et al., 2023; M. Wang et al., 2024).

151 The three GIs represent a widespread and diverse class of element in *Pseudomonas*

152 Given knowledge of shared features of the three elements, we turned to whole genome sequences and
153 asked whether *Pseudomonas* genomes harbor elements with these basic features. Search criteria
154 included the presence of *intY* downstream of *tmRNA*, as well as the presence of an *alpA*, or a 23 bp
155 sequence (TTC AGA TTA CCC CGG CTC CAC CA, the last 14 bp being the direct repeat) that is common to
156 the 3'-end of each element. Searches revealed 99 elements from 17,078 *Pseudomonas* genomes. Fig. 2a
157 shows the bioinformatic workflow and Fig. 2b depicts the relationship among the elements, constructed
158 based on previously established methods (Low et al., 2019; Nayfach et al., 2021). Briefly, 36 ORFs that
159 are commonly present in the entire set of MGEs were selected as core genes. For each element, the
160 core genes were concatenated in order, with gaps allowed where core genes are absent. The tree was
161 then inferred based on the concatenated sequences. The cladogram should be interpreted in a
162 topological sense; the edges represent evolutionary relationships only (and not distances).

163 Overall, the elements are highly diverse in terms of size and gene content (Fig. 2b). The largest elements
164 are in excess of 70 kb with the smallest being less than 20 kb. No two elements are identical; however,
165 several are highly similar. For example, the element detected in *P. rhodesiae* B21-046 (NCBI RefSeq
166 Assembly GCF_024748755.1) is 99.96% identical at the nucleotide level to I55 acquired by SBW25. As
167 described more fully below, these two host genomes are highly divergent. Other examples of such pairs
168 are denoted by pink boxes in Fig. 2b.

169 Fig. 2c lists the rank abundance of genes that occur at least 10 times across the elements, along with
170 functional classes and corresponding COG categories (Tatusov, 2000). Many elements encode
171 homologues of RadC, YqaJ, inovirus Gp2-like protein and HTH-containing protein (Fig. 2b, 2c). These are
172 also present in I23, I44 and I55 but were not included in the search criteria. Together, these genes, in
173 addition to *intY* and *alpA*, likely define core element functions. In terms of functional categories, those
174 encoding functions related to DNA replication, recombination, repair and transcription are frequently
175 represented. Furthermore, most elements contain recognizable defense systems against bacteriophages
176 (Fig. 2b). Many genes are found as singletons with 104 of the 241 functional gene classes identified via
177 matches to protein databases being represented just once (Table S6). Additionally, most elements
178 harbor at least one recognizable ORF with no matches to genes in databases (Fig. 2b).

179 To explore the relationship among elements and host genomes, a comparison of pairwise distances
180 between MGEs and hosts was performed. This involved construction of phylogenetic trees for both
181 MGEs and hosts (the latter based on 16S rDNA sequences) with the results represented in Fig. 2d. The
182 elements shown on the X- and Y- axes are ordered based on clustering shown in Fig. 2b. The region
183 above the diagonal represents similarity among elements, with the region below showing similarity
184 among hosts. For example, with focus on comparison between I55 (in *P. fluorescens* SBW25) and the
185 element in assembly GCF_024748755.1 (in *P. rhodesiae* B21-046), which is marked by a pink box: the
186 square below the diagonal is colored dark blue indicating that the two elements are highly similar. When
187 the same comparison is made above the diagonal, the corresponding box is light blue indicating that the
188 host genomes carry divergent 16S rDNA sequences. Similar patterns are evident throughout; dark blue
189 regions below the diagonal very often correspond to divergent hosts. These incongruent patterns are
190 indicative of the transfer of similar elements across a diverse range of host genomes as expected for
191 elements capable of frequent horizontal movement (Colombi et al., 2024; Koutsovoulos et al., 2022).

192 I55 is transduced by a jumbo bacteriophage present in community filtrate

193 With focus on I55, we asked whether the element is capable of autonomous transfer from one SBW25
194 cell to another. To this end, I55 was tagged with a kanamycin resistance (Kan^R) marker (strain
195 MPB39465/MPB39467). The gene encoding resistance (including promoter and a synthetic transcription
196 terminator) was inserted in the intergenic region between *orf08* and *orf09*. The location – between two
197 convergently transcribed genes – was chosen in order to minimize chances that insertion disrupted
198 element function. SBW25 carrying a chromosomally-integrated tetracycline resistance (Tet^R) gene (strain
199 MPB39500) was used as the recipient. Donor and recipient strains were co-cultured in liquid medium
200 without shaking (Fig. 3a) and on solid agar plates (as per a standard conjugation assay). No colonies
201 expressing both resistance markers were detected. This suggests that I55 is incapable of autonomous
202 intercellular movement.

203 In the original serial transfer experiment, filtrate from serially-propagated compost C had been added to
204 SBW25 cultures. We thus considered it possible that one or more components of the filtrate might be
205 necessary to mobilize the element. To this end, the experiment above was repeated in liquid medium,
206 but this time with the addition of filtrate from compost C (Fig. 3a). On plating mixtures to selective agar
207 an average ~10^4 colonies (per mL) resistant to kanamycin and tetracycline were detected (Fig. 3b).
208 Deletion of the tyrosine integrase *intY* encoded on I55, resulting in donor strain SBW25-I55Δ*intY*-Kan^R
209 (strain MPB39565/MPB39568), significantly reduced the double resistant colonies to ~10^2 colonies (per
210 mL) ($p < 0.0001$). This indicates that circularization – or linear concatenated repeats – of I55 (see Fig. E2
211 for details) underpins intercellular transfer.

212 Next, we asked whether donor-recipient cell-cell contact is necessary for the transfer of I55. To test this,
213 the transfer process was divided into two steps (Fig. 3c). In the first step, SBW25-I55-Kan^R with filtrate
214 from compost C was cultured and the filtrate collected. In the second step, recipient SBW25-Tet^R was
215 grown with addition of the filtrate obtained from the first step. The mixture was plated as previously. On
216 average, more than 10^6 colonies (per mL) resistant to both antibiotics were detected (Fig. 3d), indicating
217 that transfer of I55 is independent of cell-cell contact. However, if the compost filtrate was added at the
218 second step and not the first, then no double-resistant colonies were detected (Fig. 3d). I55 therefore
219 requires some component in the community filtrate in order to mediate transfer to recipient cells.

220 While phages are plausible facilitators of horizontal transfer, there existed the possibility that phages
221 may be indirectly involved and required solely for cell lysis. If so, then I55 would exist as naked DNA
222 during transfer and susceptible to degradation by DNase. Culture filtrate applied to the recipient culture
223 was therefore treated with DNase I, but no reduction in the number of transformants was observed (Fig.
224 3e).

225 To identify the filtrate component necessary for mobilization, serial dilutions of the community filtrate
226 were made with the aim of diluting out the transfer agent. A sample from each dilution was then used
227 as additive ① in the two-step transfer assay (Fig. 3c). In each instance a threshold was observed below
228 which no transfer occurred. Samples immediately above and below the critical limit were subject to
229 amplification and DNA sequence analysis. The resulting DNA sequence reads revealed presence of a
230 jumbo phage similar to *pPa_SNUABM_DT01* (Fig. 3f) and hereafter referred to as JPTI55. To determine
231 the correlation between presence of the JPTI55 and I55 transfer, the two-step transfer assay exploiting
232 the dilution-to-extinction design was conducted for three independent filtrate samples, each with 10
233 biological replicates at each dilution. Transfer of I55 was observed if and only if JPTI55 was detected (by
234 PCR) in the filtrate (Fig. 3g).

235 Next, we sought to isolate JPTI55 and thus confirm by direct experimentation the involvement of JPTI55
236 in transfer. To this end aliquots of community filtrate from various dilutions were plated against SBW25.
237 On standard 0.4% top-agar LB plates, morphologically uniform large plaques (LP) were detected, but
238 these plaques were present at dilutions lower than those that resulted in I55 transfer. Moreover, PCR
239 analysis of plaques using primers diagnostic for JPTI55 proved negative. Attempts to transfer I55 to new
240 hosts via addition of phages purified from these plaques also proved negative.

241 The experiment was therefore repeated but plating was performed on SBW25 contained in 0.2% top-
242 agar M9-glucose plates. At this reduced agar concentration – and at dilutions corresponding to those in
243 which JPTI55 was known to be present in the filtrate – two morphologically distinct plaques were
244 observed. PCR analysis confirmed that the small clear (less abundant) plaques (see Fig. 3h) contained
245 JPTI55.

246 Individual plaques were subject to three rounds of purification by plaque assay. Finally, the two-step
247 transfer assay was conducted with JPTI55 and/or LP phages added to donor or recipient cultures. The
248 results (Fig. 3i) demonstrate that JPTI55 was solely responsible for the transfer of I55 – and did so as
249 efficiently as the culture filtrate from which it was isolated.

250 To directly test whether I55 behaves as a phage satellite, we assessed whether the jumbo phage JPTI55
251 could non-specifically package host DNA. If I55 were transferred simply as part of generalized
252 transduction, chromosomal markers unrelated to I55 would also be detected among transductants. We

253 engineered SBW25 strains carrying chromosomal (strain MPB29284) and plasmid-borne (strain
254 MPB16791) antibiotic resistance markers, and repeated the two-step transfer assays with purified
255 JPTI55. No transfer of chromosomal or plasmid markers was observed (Fig. 3j), indicating that
256 generalized transduction does not occur (or is below the detection limit). These findings suggest that I55
257 is preferentially packaged and transferred by JPTI55 in a manner consistent with the behavior of a phage
258 satellite (Penadés et al., 2025).

259 A type II restriction-modification system protects against UFV-like phages

260 We next sought understanding of the fitness consequences of element carriage and again focused
261 attention on I55. I55 encodes several putative phage defense systems (*orf02*, *orf17*, *orf24*, *orf37*), and
262 compost filtrate is rich in phages (Quistad et al., 2020). We therefore hypothesized that I55 confers a
263 fitness benefit to its host by providing resistance against phages. By fluorescence-based competition
264 assays (Fig. 4a), the data show that I55 confers a significant fitness advantage (~6%) in the presence of
265 compost filtrate (p = 0.0104), but is costly (~2%) in the absence of the filtrate (p = 0.0033) (Fig. 4b). To
266 directly test the hypothesis that the benefit of I55 carriage arises from phage protection, compost C
267 filtrate was plated against lawns of SBW25 and of SBW25 carrying I55. Plaques were observed on both
268 hosts, but carriage of I55 significantly reduced infection and cell lysis (Fig. 4c).

269 Five phages – all with the LP morphology – were purified from single plaques on plates shown in Fig. 4c.
270 Whole genome sequencing revealed the phages to be identical at the nucleotide level. Interrogation of
271 the phage genome against NCBI databases showed that the closest relative is *Pseudomonas* phage UFV-
272 P2 (Fig. 4d). Henceforth we refer to phages from large plaques as UFV-like phages. The fluorescence-
273 based competition assay was then repeated with pure UFV-like phages, and the assay result was
274 qualitatively reproduced (see Fig. 4e). This shows that defense against UFV-like phage present in the
275 community filtrate partially explains the fitness benefit of I55.

276 To determine regions of I55 responsible for protection against the UFV-like phages, the element I55 was
277 divided into six regions (RTBD01-06, see Fig. 4f) according to operon structures, and each region was
278 separately deleted (strains MPB42170, MPB41585, MPB42372, MPB42031 and MPB41438, for
279 Δ*RTBD02*, Δ*RTBD03*, Δ*RTBD04*, Δ*RTBD05* and Δ*RTBD06*, respectively). Spot assay with UFV-like phages
280 revealed that deletion of the sixth region (RTBD06) abolished the phage defense phenotype of I55, while
281 deletions of the other five regions (except RTBD01, which we were unable to construct) maintained
282 defense level of intact I55 (Fig. 4f). DefenseFinder predicts *orf37*, encoded within region RTBD06, to be a
283 type II-G restriction-modification system. We thus deleted *orf37* – producing SBW25-I55Δ*intY*Δ*orf37*
284 (strain MPB42855) – and repeated the spot assay, and observed infection levels comparable to SBW25.
285 This confirmed that the phage defense phenotype of I55 is encoded by *orf37*.

286 Finally, we tested whether *orf37* is indeed the cause of the fitness benefit of I55 in environments with
287 community filtrate or UFV-like phages. Fluorescence-based competition assays were conducted with
288 SBW25-I55Δ*intY*Δ*orf37* against SBW25-I55Δ*intY*. As expected, deletion of *orf37* significantly reduced
289 host fitness in presence of community filtrate or UFV-like phages (p = 0.0035 and 0.0014, respectively,
290 see Fig. 4g), but had no fitness influence in the absence of both (p = 0.4237), which supported the
291 hypothesis that the fitness effect of I55 is explained by *orf37*. Competition of SBW25-I55Δ*intY*Δ*orf37*
292 against the wild type SBW25 showed that the former was always slightly less fit than the latter
293 regardless of the environment (p = 0.0331, 0.0252 and 0.0008, in environments with community filtrate,
294 with UFV-like phages and with no additives, respectively).

295

296 Discussion

297 Horizontal gene transfer (HGT) mediated by mobile genetic elements (MGEs) shapes the diversity and
298 function of microbial communities, but much remains to be discovered regarding both the vehicles of
299 transfer and the functional genes subject to horizontal movement. The study reported here, was
300 motivated by earlier work (Quistad et al., 2020), in which repeated exposure of compost community
301 filtrates to fresh bacterial hosts caused a substantial fraction of community DNA to enter the
302 horizontally disseminated pool. Comparative metagenomics revealed genes of ecological significance
303 and, in some cases, known MGEs such as phages and plasmids. However, progress has been constrained
304 by the inability to experimentally capture unknown elements in culturable hosts.

305 Here, we simplified the original strategy: we retained the complexity of community-derived filtrates but
306 exposed these to a single, genetically tractable strain of *Pseudomonas fluorescens*. Within a short
307 period, the focal bacterium acquired three MGEs – designated I23, I44, and I55 – each integrating
308 immediately downstream of the *tmRNA* gene, but lacking typical structures indicative of autonomous
309 movement (Camargo et al., 2023; de Sousa et al., 2023; Néron et al., 2023; M. Wang et al., 2024; Xie &
310 Tang, 2017). Using minimal defining features – target site, 3'-end sequence, and integrase – we
311 identified ~100 related elements within *Pseudomonas*, though the class is broader. Relaxing constraints
312 on flanking sequence similarity revealed that elements with essential features of the three MGEs are
313 widespread. Many such genomic islands insert at *tmRNA* or *tRNA* genes, are flanked by direct repeats,
314 encode tyrosine recombinases, and lack genes for autonomous transfer. The "phage defense elements"
315 recently described by (Hussain et al., 2021) exemplify this class. Moreover, Islander (Hudson et al.,
316 2015), a tool for detecting integrases downstream of *tmRNA*/*tRNA*, shows that similar elements are
317 present across both eubacteria and archaea.

318 Starting from evidence that I55 is incapable of autonomous transfer, we hypothesized the involvement
319 of a helper element (Ares-Arroyo et al., 2024). The occurrence of I55 transfer in the absence of cell–cell
320 contact and despite DNase treatment pointed to a phage-mediated mechanism. Using dilution-to-
321 extinction assays on filtrates, we linked transfer to the presence of a jumbo bacteriophage, JPTI55.
322 Further experiments revealed that I55 is transduced by JPTI55 as a satellite – a finding that, to our
323 knowledge, is the first report of a phage satellite parasitizing a jumbo phage.

324 The SBW25–I55–JPTI55 system opens new avenues for exploring unconventional mechanisms of gene
325 transfer and for developing tools for genetic engineering. Most known phage satellites parasitize phages
326 with genomes under 200 kb (Penadés et al., 2025), whose replication and packaging occur in the
327 cytoplasm. In contrast, jumbo phages form proteinaceous shells that enclose replicating DNA in the
328 cytoplasm (Laughlin et al., 2022), potentially creating a barrier to satellite hijacking. That I55 can bypass
329 or penetrate this structure suggests novel biology. Additionally, the known size constraints of standard
330 phage capsids limit satellites to ~20 kb, restricting their use as vectors. With I55's larger genome and its
331 association with the large JPTI55 capsid, the possibility arises for shuttling larger cargo between cells.
332 However, identifying the minimal satellite backbone, host range and methods for phage elimination is a
333 prerequisite for realizing this potential.

334 Beyond I55's mode of transfer, its experimental capture provides a paradigm for uncovering MGE
335 mobility in complex environments. A similar approach may help resolve the mystery surrounding the

336 ~41 kb *Vibrio* Pathogenicity Island-1 (VPI-1), which encodes the toxin-coregulated pilus receptor for
337 CTXΦ, the cholera toxin phage. VPI-1 acquisition enables subsequent CTXΦ entry and conversion of
338 environmental *Vibrio cholerae* into toxigenic strains (Faruque & Mekalanos, 2003, 2012). Although VPI-1
339 is known to have transferred horizontally (Karaolis et al., 1999; O'Shea & Boyd, 2002), its mobility
340 remains controversial (Faruque et al., 2003). A protocol akin to that used to identify JPTI55 may lead to
341 identification of a secondary transfer agent – possibly also a jumbo phage – providing a strategy to block
342 transmission.

343 A benefit of working with I55 in a genetically tractable host was the ability to determine fitness effects.
344 Acquisition of I55 conferred a clear advantage in the presence of compost filtrate (but a small cost in its
345 absence), explaining its detection in the limited number of sequenced colonies arising from the initial
346 selection experiment. The benefit appears to stem in part from phage defense. Experiments with UFV-
347 like phages purified from filtrate confirmed I55's protective effect. Systematic deletions identified *orf37*,
348 a type II restriction-modification system, as responsible for resistance to UFV-like phages. Other
349 predicted phage defense systems in I55 – including dynamin and RecBCD orthologs (Dillingham &
350 Kowalczykowski, 2008; Guo et al., 2022) – were not active against these phages, but could function in
351 other contexts. More generally, this finding supports the view that MGEs are reservoirs of phage
352 defense systems, which enhance their own propagation (Bernheim & Sorek, 2020; Hussain et al., 2021;
353 Johnson et al., 2023; Rousset et al., 2022).

354 The discovery of I55-family elements and their JPTI55-mediated mobilization exposes a previously
355 hidden layer of HGT involving jumbo phages and satellites. While the elements described here represent
356 only a fraction of the diversity likely present, they highlight how microbial communities can facilitate
357 gene flow at scales reminiscent of sexual reproduction in eukaryotes (Rainey & Quistad, 2020). Applying
358 this experimental strategy to other hosts and habitats is likely to uncover further mobile elements, novel
359 gene cargos, and distinct transfer mechanisms – critical for understanding the ecological and
360 evolutionary forces that shape microbial communities.

361 # Materials and Methods

362 ## Strains and growth conditions

363 All bacterial strains used in this study are listed in Table S1. All strains were preserved in -80 °C with 30%
364 glycerol saline.

365 *Isolation of foreign elements, plasmid construction, strain construction*: Unless otherwise stated, *P.*
366 *fluorescens* SBW25 strains were cultured in LB-Miller (LB) broth at 28 °C, while *E. coli* strains were
367 cultured in LB (with antibiotics where maintenance of plasmids was required) at 37 °C, both shaking at
368 220 rpm for 16-24 h.

369 *Experimental evolution, intercellular transfer assay and fluorescent fitness assay*: Unless otherwise
370 stated, each pre-conditioning and incubation was performed in the absence of shaking at 28 °C, in 5 mL
371 freshly made M9-glucose medium (M9 salt solution supplemented with 2 mM $MgSO_4$, 0.1 mM $CaCl_2$ and
372 0.2% w/v D-glucose) in a 15 mL Falcon tube.

373 *Plaque assay and bacteriophage isolation*: All assays were done in S-LB environment, except the assay
374 for isolation of the jumbo phage JPTI55 (see below) which was done in M9-glucose environment. For the
375 S-LB environment, unless otherwise stated, bacterial host strains were cultured in S-LB medium (LB
376 medium supplemented with 10 mM $MgCl_2$ and 5 mM $CaCl_2$) at 28 °C, shaking at 220 rpm for 16-24 h
377 until stationary phase. The semi-soft agar (SSA) used consisted of S-LB medium and 0.4% agar. The
378 bottom agar consisted of LB medium and 1.5% agar. For the M9-glucose environment, unless otherwise
379 stated, bacterial host strains were cultured in M9-glucose medium at 28 °C, shaking at 220 rpm for 16-
380 24 h until stationary phase. The semi-soft agar (SSA) used consisted of M9-glucose medium and 0.2%
381 agar. The bottom agar consisted of M9-glucose medium and 1.5% agar.

382 Bacterial culture was plated on respective growth medium supplemented with 1.5% agar. Unless
383 otherwise stated, agar plates were incubated at 28 °C. Antibiotics were applied as per the following
384 concentrations: kanamycin (Kan, 50 µg/mL), nitrofurantoin (100 µg/mL), tetracycline (Tet, 12.5 µg/mL),
385 gentamicin (Gm, 20 µg/mL), *Pseudomonas* CFC selective supplement (Millipore, as per the manual).

386 ## Compost community sampling, storage and retrieval

387 Three heaps of garden compost, named B, C and D, were sampled within 10 km of Plön, Germany
388 (54°9'44"N, 10°25'17"E), from May to August 2022. Upon collection, the samples were immediately
389 transferred to laboratory and processed as following. For each sample, 30 g compost was mixed with
390 150 mL M9 salt solution, shaken vigorously for ~30 sec, and left static for ~5 min. The supernatant was
391 distributed into 1 mL aliquots, to each of which 350 µL glycerol saline was added. The aliquots were
392 frozen in -80 °C for storage.

393 To retrieve the compost wash, one aliquot from the frozen stock was kept on ice for ~10 min. After
394 thawing, the mixture was pelleted by centrifuging at 15000 rcf for 1 min, resuspended in 1 mL M9 salt
395 solution, and then pelleted by centrifuging again. The washed pellet was then resuspended in 500 µL M9
396 salts solution to inoculate microcosms.

397 ## Community filtrate (fixed) generation, storage and retrieval

398 Initially, 500 µL washed suspension from one compost wash aliquot was inoculated into 100 mL M9-
399 glucose medium in a 500 mL microcosm. The microcosm was incubated without shaking at 28 °C for 7

400 days. At the end of incubation period, the whole culture was filtered with a 0.2 µm filter (Whatman).
401 The filtrate was distributed into 600 µL aliquots. Aliquots were directly frozen at -80 °C for storage.

402 To retrieve the community filtrate, one aliquot from the frozen stock was kept at room temperature for
403 ~10 min. After thawing, the aliquot was directly used to inoculate microcosms. Unless otherwise stated,
404 50 µL community filtrate was added to each microcosm.

405 As a negative control, *P. fluorescens* SBW25 was used in place of the washed suspension, and otherwise
406 followed exactly the same generation, storage and retrieval protocols to obtain the SBW25 filtrate to
407 inoculate microcosms.

408 Experimental evolution

409 *Co-culture regime*

410 Parallel lines of SBW25, cocultured with the compost community, were serially propagated. In detail,
411 SBW25-RFP-Gm^R (strain MPB28806) and 90 µL washed suspension from compost C were inoculated.
412 There were three parallel lines, with one control line where no washed suspension was added. For each
413 line, an 1/20 transfer was made every 24 h, for a total of five transfers. At each transfer, a dilution series
414 of the culture was spread plated on LB + CFC + Gm plates, which were then cultivated for 24 h. The
415 number of RFP colonies were counted and recorded.

416 *Fixed filtrate regime*

417 Parallel lines of SBW25 were serially propagated, with aliquots of filtrate from the frozen stock added at
418 each transfer. In detail, filtrate from communities B, C and D, and from SBW25, were separately used.
419 For each type of filtrate, there were five parallel lines of SBW25-GFP-Kan^R (strain MPB29284) and five
420 parallel lines of SBW25-RFP-Kan^R (strain MPB29300). For each line, an 1/100 transfer was made every 48
421 h, for a total of seven transfers. At each transfer, 50 µL filtrate was added to a fresh microcosm, and
422 aliquots from the old microcosm were stored at -80 °C.

423 *Live filtrate regime*

424 Parallel lines of SBW25 were serial propagated, with aliquots of filtrate from independently propagated
425 communities or SBW25 added at each transfer. In detail, 200 µL washed suspension from compost C
426 wash was added and transferred 1/100 every 48 h, yielding fresh filtrate by filtering 1mL of the culture
427 through a 0.2 µm filter (Whatman). As a negative control, *P. fluorescens* SBW25 was used in place of the
428 washed suspension, but otherwise the same protocol was followed to obtain SBW25 filtrate. At the
429 same time, for each type of filtrate, there were four parallel lines of SBW25-GFP-Kan^R (strain MPB29284)
430 and four parallel lines of SBW25-RFP-Kan^R (strain MPB29300). For each line, a 1/100 transfer was made
431 every 48 h, for a total of 14 transfers. At each transfer, 50 µL fresh filtrate was added to the new
432 microcosm, and a sample from the old microcosm were stored at -80 °C.

433 PCR and gel electrophoresis

434 All PCR primers used in this study are listed in Table S3. PCR was done with NEB Q5 polymerase, with
435 either extracted DNA or bacterial suspension as templates. Annealing temperatures and extension time
436 was determined as per NEB Tm Calculator (version 1.16.6). Unless otherwise stated, 35 cycles were
437 performed. Gel electrophoresis was performed for 5 µL PCR products with 1x DNA loading dye, in 1%
438 agarose gels.

Detection, isolation and annotation of foreign elements

For each line, frozen culture at the last transfer was serially diluted and plated out on LB plates. For the live-filtrate regime, 2 to 3 colonies were picked and separately cultured overnight, from which aliquots were frozen and DNA extracted with Qiagen DNeasy UltraClean Microbial kit. DNA samples were sequenced by Illumina NextSeq for at least 300x coverage. For fixed-filtrate regime, 24 colonies were randomly picked and cultured up overnight in 300 µL LB in 96-deep-well plates. Aliquots from each of the 24 cultures were mixed in equal proportion and then DNA extractions were performed with Qiagen DNeasy UltraClean Microbial kit. The leftovers in 96-deep-well plates were stored at -80 °C. DNA samples were Illumina short-read sequenced (read length 150 bp) by Eurofins Scientific SE for at least 300x coverage.

Bioinformatic analysis of sequencing data was done in Geneious Prime 2022.2.1 (https://www.geneious.com). For each sample, raw reads were trimmed by BBDuk and mapped to *P. fluorescens* SBW25 reference genome (Fortmann-Grote et al., 2023) under the default settings. The unmapped reads were saved and then *de novo* assembled. The vast majority of contigs were short (< 1 kb) and apparently artefacts of sequencing technology. However, in some samples, long (> 10 kb) and good quality contigs were obtained. To test if the contig inserted into the genome as a foreign element, the first 50 bp and last 50 bp of the contig were blasted against the reference genome. If the two regions mapped, manual comparison were used to confirm the insertion and its locus.

To confirm the insertion of the foreign element, two primer pairs were designed, flanking either the left or the right junction of the insertion. For fixed-filtrate regime, the two primer pairs were additionally used to exclude the cultured isolates (out of the 24 picked) that carried the foreign element. Such isolates were then routinely whole-genome sequenced by Eurofins Scientific SE and Variations / SNPs calling was subsequently performed. Table S5 shows the list of mutations detected in each isolate.

The three foreign elements were screened for open reading frames (ORFs) by Prokka (Seemann, 2014) in KBase (Arkin et al., 2018). The ORFs were then annotated by Pfam in InterProScan (Jones et al., 2014). The elements were also screened by DefenseFinder (Tesson et al., 2022) for potential phage defense systems. Alignment of the 3 foreign elements was done by Easyfig (M. J. Sullivan et al., 2011) based on blastn under the default settings.

Detection and analysis of similar elements in databases

The nucleic acid sequences of the *tmRNA*, *intY* (from the element I55) and the 23 bp sequence at the 3'-end were compared to representative genomes in GTDB-tk (version R214) (Chaumeil et al., 2020). Sequence comparisons revealed that 35 representative genomes contain all three sequences, and they all belong to the family *Pseudomonadaceae*. This motivated a more focused and thorough search within this family. Therefore, the nucleic acid sequences of the *tmRNA*, *intY* (from the element I55) and the 23 bp sequence at the 3'-end were compared to all available genomic sequences (17,078 in total) of strains belonging to the family *Pseudomonadaceae*. Sequence comparisons revealed that 136 genomes in the family *Pseudomonadaceae* contain all three sequences. Those 136 genomes were then subject to gene prediction by Prodigal (v2.6.3) (Hyatt et al., 2010) and functional annotation by eggNOG-mapper (v2) (Cantalapiedra et al., 2021). Based on annotations, 99 genomes fulfilled the following criteria: (1) contained an annotated tmRNA; (2) contained an annotated tyrosine integrase (IntY); (3) contained at least one of an annotated AlpA or the 23 bp sequence. These 99 genomes are derived from 67 species, all in the genus *Pseudomonas*. In each genome, the MGEs were isolated by extracting the sequence from

481 the 3'-end of the *tmRNA* to the 3'-end of the 23 bp sequence or the 3'-end of *alpA*. All MGEs were
482 screened by DefenseFinder (Tesson et al., 2022) for potential phage defense systems.

483 To establish evolutionary relationships of the 99 detected MGEs and I23, I44 and I55, a cladogram of the
484 102 MGEs was built based on previously established methods (Low et al., 2019; Nayfach et al., 2021).
485 Briefly, 36 ORFs that are commonly present in the MGEs were selected as marker genes. For each MGE,
486 the marker genes were concatenated in order, with a gap introduced in cases where a marker gene was
487 absent. The tree of the MGEs was then inferred based on the concatenated sequences.

488 To assess host-MGE relationships, the 16S rDNA sequences of the hosts of the 102 MGEs were
489 extracted. Among them, 5 host genomes lack detectable 16S rDNA regions and hence were excluded
490 from the following analysis. For the 97 remaining genomes, phylogenetic trees were built separately
491 based on the 16S rDNA sequences by Clustal (v2.1) (Sievers et al., 2011), and based on the MGE
492 sequences by the same method as before (Low et al., 2019; Nayfach et al., 2021). The two trees were
493 converted to distance matrices in R (version 4.1.2), with rows clustered according to MGE distances.

494 Plasmid construction

495 All plasmids used in this study are listed in Table S2. Plasmid pUIsacB (plasmid MPB35522) backbone
496 was amplified by PCR. SBW25 genomic fragments flanking the region of interest, where a mutagenesis,
497 knock-out or knock-in was to be performed, were amplified by PCR. In particular, the Kan^R fragment
498 used to tag I55 was produced by cloning the Kan^R gene from plasmid pMRE-Tn*7*-152 (plasmid
499 MPB27708) followed by a synthetic transcription terminator (CCA ATT ATT GAA CAC CCT TCG GGG TGT
500 TTT TTT GTT TCT GGT CTC CC). Primers were designed with a 5' overhang to facilitate assembly.
501 Backbone and fragments were assembled (with NEBuilder HiFi DNA Assembly Master Mix) and
502 transformed into *E. coli* Top10 competent cells. Successful transformants were selected on LB + Tet
503 plates, and confirmed by PCR and Sanger sequencing across the construct.

504 Strain construction

505 *Two-step allelic replacement (2SAR)*

506 The method is adapted from Hmelo et al. (Hmelo et al., 2015) and extensively described by Farr et al.
507 (Farr et al., 2025). Briefly, recipient (*P. fluorescens* SBW25), donor (*E. coli* carrying the plasmid used for
508 allelic exchange) and helper (*E. coli* carrying plasmid pRK2013, plasmid MPB35623) strains were cultured
509 overnight until stationary phase. Then, 1 mL recipient culture was heat-shocked at 42 °C for 20 min, and
510 subsequently mixed with 500 µL donor and 500 µL helper culture. The mixture was pelleted and
511 resuspended in 100 µL LB, which was then spotted onto an LB plate for incubation overnight. The
512 cultivated cell layer was then plated out on an LB + nitrofurantoin + Tet plate and incubated overnight to
513 select for trans-conjugates. Single trans-conjugates were then picked and streaked onto TYS10 plates,
514 which were subsequently incubated overnight. Finally, PCR and Sanger sequencing were used to screen
515 for the desired mutants.

516 *Fluorescent tagging*

517 The method is adapted from Schlechter et al. (Schlechter et al., 2018). Briefly, recipient (*P. fluorescens*
518 SBW25) and donor (*E. coli* carrying the plasmid pMRE-Tn*7*-152 or pMRE-Tn*7*-155, MPB27708 or
519 MPB27709, respectively) strains were cultured overnight until stationary phase. Then, 1 mL recipient
520 culture was heat-shocked at 42 °C for 20 min, and subsequently mixed with 1 mL donor culture. The
521 mixture was pelleted and resuspended in 100 µL LB, which was then spotted onto an LB plate for

522 incubation overnight. The cultivated cell layer was then plated out on an LB + nitrofurantoin + Kan +
523 0.1% w/v arabinose plate and incubated overnight to select for trans-conjugates. Single trans-conjugates
524 were picked, and integration of the fluorescent tag was then confirmed by PCR.

525 *Preparation of* SBW25-I55 *and* SBW25 *(reconstructed) for assays*

526 DNA sequencing of the evolved isolate carrying I55 (strain MPB33357) revealed, in addition to presence
527 of the mobile element, two SNPs elsewhere in the genome (see Table S5) that had arisen during the
528 course of serial propagation. Additionally, this isolate also harbored the Tn*7*-152 cassette. While there
529 was no reason to suspect any connection to I55, these SNPs were reverted to the ancestral SBW25
530 sequence, and Tn*7*-152 removed, by site-directed mutagenesis using the 2SAR strategy described above.
531 Prior to these mutagenesis steps, two independent colonies were picked from the evolved isolate and
532 treated as biological replicates in all subsequent genetic manipulations. The resulting genotype, SBW25-
533 I55 (strain MPB39024/MPB39026) is in principle isogenic with SBW25 (strain MPB29212). However, to
534 be more certain of this fact, the ancestral SBW25 genotype used in the fitness assays and plaque assays
535 was re-generated from SBW25-I55 by removal of the element, giving reconstructed SBW25 (strain
536 MPB39379/MPB39459).

537 Intercellular transfer assay

538 *Conjugation regime*

539 The donor, a SBW25 strain with Kan^R-tagged I55 (strain MPB39465/MPB39467), recipient, a SBW25
540 strain with a Tet^R marker (strain MPB39500), and helper, *E. coli* carrying plasmid pRK2013 (plasmid
541 MPB35623), were cultured overnight until stationary phase. Then, 1 mL recipient culture was heat-
542 shocked at 42 °C for 20 min, and subsequently mixed with 500 µL donor and 500 µL helper culture. The
543 mixture was pelleted and resuspended in 100 µL LB, which was then spotted onto an LB plate for
544 incubation overnight. The cultivated cell layer was then plated out on an LB + Kan + Tet plate and
545 incubated overnight to select for trans-conjugates.

546 *One-step regime*

547 The donor, a SBW25 strain with a Kan^R-tagged I55 (with or without *intY*, strains MPB39465/MPB39467
548 or MPB39565/MPB39568, respectively), and the recipient, a SBW25 strain with a Tet^R marker (strain
549 MPB39500), were cultivated separately for 48 h for pre-conditioning. Then 25 µL of each culture and 50
550 µL of community filtrate from frozen stocks (autoclaved or not) were inoculated into the same
551 microcosm and then cultivated for a further 48 h. A dilution series of the culture was then spread plated
552 on LB + Kan + Tet plates, which were then cultivated for 24 h. The number of colonies were counted and
553 recorded.

554 *Two-step regime*

555 For the first step, the donor, a SBW25 strain with a Kan^R-tagged I55 (or its derivatives), were cultivated
556 for 48 h for pre-conditioning. Then 50 µL of the donor culture, with 5 µL additives (called additive ①)
557 where applicable, was added to microcosms and then cultivated for a further 48 h. A stock of donor-
558 culture filtrate was obtained by filtering the culture through a 0.2 µm filter (Whatman). The filtrate was
559 distributed into 100 µL aliquots. Aliquots were directly frozen in -80 °C for storage. To retrieve the
560 donor-culture filtrate, one aliquot from the frozen stock was kept at room temperature for ~10 min.

561 For the second step, the recipient, a SBW25 strain with a Tet^R marker (strain MPB39500), was cultivated
562 for 48 h for pre-conditioning. Then 50 µL of the recipient culture, with 5 µL donor culture filtrate (from

563 the stock generated in the first step of the assay, and treated before use where applicable), and with 5
564 µL additives (called additive ②) where applicable, was added to microcosms and then cultivated for a
565 further 48 h. To test the presence of transfer events of I55, 3 µL of the culture was spotted on LB + Kan +
566 Tet plates, which were then cultivated for 24 h before pictures were taken. To quantify the density of
567 recipient cells that received I55, a dilution series of the culture was spread plated on LB + Kan + Tet
568 plates, which were then cultivated for 24 h before the number of colonies was recorded. To estimate
569 the proportion of recipient cells that received I55, a dilution series of the culture was spread plated on
570 LB + Kan + Tet plates and on LB + Tet plates, which were then cultivated for 24 h before the number of
571 colonies was recorded and divided for proportion.

572 In the first step, the additive ① was in general community filtrate from the stock of the 'fixed' regime,
573 or pure bacteriophage lysates. In cases where the density of agents that were capable of transferring I55
574 (but not necessarily carrying I55 at this point) in the additive ① was to be estimated, a dilution series of
575 the additive was made and used as separate treatments (called a dilution-to-extinction treatment). In
576 the second step, the additive ② was in general community filtrate from the stock of the 'fixed' regime,
577 or pure bacteriophage lysates. In cases where the density of agents that were carrying I55 in the donor
578 culture filtrate or additive ② was to be estimated, a dilution series of the filtrate or additive was made
579 and used as separate treatments (called a dilution-to-extinction treatment). Where applicable, the
580 additives and filtrate samples in first and / or second steps were treated with RNase-Free DNase I
581 (Norgen) or autoclaved before used in the assay.

582 ## Fluorescent fitness assay

583 The protocol was adapted from Barnett et al. (Barnett et al., 2025). Two competitor strains, one with a
584 GFP tag and the other with an RFP tag, were cultivated separately for 48 h for pre-conditioning. Then 25
585 µL of each culture, and additives (50 µL of community filtrate or 2 µL of phage lysate, see following
586 sections) from frozen stocks were inoculated into the same microcosm (with 5 mL fresh medium), which
587 was then cultivated for a further 48 h. At the beginning and end of the second incubation period, the
588 ratios of GFP to RFP cells were determined by flow cytometry (MACSQuant VYB), denoted by r_0 and r_1,
589 and total densities of cells in the microcosm were determined by spread plating on LB plates, denoted
590 by n_0 and n_1. The relative fitness of GFP to RFP cells is the ratio of Malthusian parameters (Lenski et al.,
591 1991), given by

592 $$1 + \frac{\log\left(\frac{r_1}{r_0}\right)}{\log\left(\frac{n_1(1+r_0)}{n_0(1+r_1)}\right)}.$$

593 The relative fitness of RFP to GFP cells is the reciprocal of the above expression. To eliminate any fitness
594 difference due to the choice of fluorescent protein markers, the reverse tagging strategy of the two
595 competitor strains with fluorescent protein markers was also implemented to calculate relative fitness.

596 ## Filtrate sequencing and analysis

597 To sequence each culture filtrate sample, a 100 µL aliquot of filtrate was extracted with Norgen Phage
598 DNA Isolation kit. The concentrations of eluted DNA were in general lower than ~1 ng/µL and
599 insufficient for subsequent sequencing. To amplify the DNA, 10 µL of eluted DNA was amplified with
600 Cytiva GenomiPhi V3 Ready-To-Go DNA Amplification kit. The amplified DNA was extracted again with
601 Qiagen QIAquick PCR purification kit. The DNA samples Illumina short-read sequenced (read length 150

602 bp) by Eurofins Scientific SE for ~15M paired-end reads. Bioinformatic analysis of sequencing data was
603 done in Geneious Prime 2022.2.1 (https://www.geneious.com). For each sample, raw reads were
604 trimmed by BBDuk, and the trimmed reads were also *de novo* assembled by the assembler MEGAHIT (Li
605 et al., 2015)

606 Plaque and spot assays of bacteriophages

607 To determine the phage titer, a dilution series of community filtrate or phage lysate (see following
608 sections) was made. For plaque assays, 50 µL diluted material and 100-400 µL bacterial host overnight
609 culture were mixed into 4 mL SSA (kept at 55 °C). The mixture was immediately poured onto a plate,
610 dried in a laminar flow cabinet for a few minutes, before being incubated for ~ 36 h. For spot assays,
611 100-400 µL bacterial host overnight culture were added into 4 mL SSA (kept at 55 °C). The mixture was
612 immediately poured onto a plate and dried in a laminar flow cabinet for a few minutes. Then 3 µL of
613 diluted material was spotted onto the plate and dried in a laminar flow cabinet for another few minutes,
614 before being incubated for ~ 36 hrs. For both assays, the number of plaques or presence of
615 bacteriophage spots were determined after incubation. Pictures of the plates were taken with Bio-Rad
616 ChemiDoc Imager, under the colorimetric setting with exposure time 0.1 sec.

617 Bacteriophage isolation, storage and sequencing

618 To purify phages from the community filtrate, a plaque assay (in LB environment) using the filtrate was
619 performed. A single isolated plaque was then picked, with which a plaque assay was then performed.
620 This was repeated at least three times. Finally, a single isolated plaque from the last assay was picked
621 and amplified in exponential-phase bacterial host culture in LB medium for ~6 h. The obtained phage
622 lysate was chloroform extracted and stored in -80 °C.

623 To purify the JPTI55 jumbo bacteriophage from culture filtrate samples (see Results for details), a plaque
624 assay (in M9-glucose environment) using the filtrate was performed. Single isolated plaques were
625 randomly picked and screened for the JPTI55 genome by PCR. Another plaque assay was then
626 performed with those plaques that were formed by JPTI55. This was repeated at least three times.
627 Finally, a single isolated plaque from the last assay was picked and amplified in exponential-phase
628 bacterial host culture in M9-glucose medium for ~72 h. The obtained phage lysate was filtered through
629 0.2 µm filter (Whatman) and stored in -80 °C.

630 Amplification of all phage isolates was done by inoculating an aliquot of frozen phage lysate into
631 exponential-phase SBW25 culture in M9-glucose medium. After incubation for ~72 h, the culture was
632 filtered through 0.2 µm filter (Whatman). The filtrate was then aliquoted and directly stored in -80 °C.

633 For sequencing of the phage isolates, 500 µL frozen phage lysate was extracted by Norgen Phage DNA
634 Isolation kit. The DNA samples were then Illumina short-read sequenced (read length 150 bp) by
635 Eurofins Scientific SE for ~15M paired-end reads. Bioinformatic analysis of sequencing data was done in
636 Geneious Prime 2022.2.1. For each sample, raw reads were trimmed by BBDuk and mapped to *P.*
637 *fluorescens* SBW25 reference genome under the default settings. The unmapped reads were saved and
638 then *de novo* assembled into a circular contig. The obtained contig was blasted (Camacho et al., 2009)
639 for similar records in database, from which a phylogeny of its close relatives was built by VICTOR (Meier-
640 Kolthoff & Göker, 2017).

641 ## Statistical analysis

642 All experiments were done for at least 3 independent biological replicates. Statistical analyses were
643 performed with GraphPad Prism (v. 10.1.2). Welch's *t*-test and Mann-Whitney test were performed for
644 parametric and non-parametric pairwise comparisons, respectively.

Miscellaneous

Data availability

Supporting information, including sequencing raw reads, new reference sequences, phage sequences, and bioinformatic codes will be deposited in Edmond (https://edmond.mpg.de/).

Author contributions

Y.Z., A.D.F., D.W.R. and P.B.R. designed research; Y.Z., Y.M. and C.V. performed research; Y.Z., Y.M., A.D.F., D.W.R. and P.B.R. analyzed data; and Y.Z. and P.B.R. wrote the paper; all authors approved the final version.

Acknowledgements

We acknowledge the Max Planck Society for generous core funding. We thank members of Department of Microbial Population Biology (past and present) for support, technical assistance and discussion.

Competing interests

The authors declare no competing interest.

References

Ares-Arroyo, M., Coluzzi, C., Moura de Sousa, J. A., & Rocha, E. P. C. (2024). Hijackers, hitchhikers, or co-drivers? The mysteries of mobilizable genetic elements. *PLOS Biology*, *22*(8), e3002796. https://doi.org/10.1371/journal.pbio.3002796

Arkin, A. P., Cottingham, R. W., Henry, C. S., Harris, N. L., Stevens, R. L., Maslov, S., Dehal, P., Ware, D., Perez, F., Canon, S., Sneddon, M. W., Henderson, M. L., Riehl, W. J., Murphy-Olson, D., Chan, S. Y., Kamimura, R. T., Kumari, S., Drake, M. M., Brettin, T. S., … Yu, D. (2018). KBase: The United States Department of Energy Systems Biology Knowledgebase. *Nature Biotechnology*, *36*(7), 566–569. https://doi.org/10.1038/nbt.4163

Arnold, B. J., Huang, I.-T., & Hanage, W. P. (2022). Horizontal gene transfer and adaptive evolution in bacteria. *Nature Reviews Microbiology*, *20*(4), 206–218. https://doi.org/10.1038/s41579-021-00650-4

Barcia-Cruz, R., Goudenège, D., Moura de Sousa, J. A., Piel, D., Marbouty, M., Rocha, E. P. C., & Le Roux, F. (2024). Phage-inducible chromosomal minimalist islands (PICMIs), a novel family of small marine satellites of virulent phages. *Nature Communications*, *15*(1), 664. https://doi.org/10.1038/s41467-024-44965-1

Barnett, M., Meister, L., & Rainey, P. B. (2025). Experimental evolution of evolvability. *Science*, *387*(6736), eadr2756. https://doi.org/10.1126/science.adr2756

Bernheim, A., & Sorek, R. (2020). The pan-immune system of bacteria: Antiviral defence as a community resource. *Nature Reviews Microbiology*, *18*(2), 113–119. https://doi.org/10.1038/s41579-019-0278-2

Camacho, C., Coulouris, G., Avagyan, V., Ma, N., Papadopoulos, J., Bealer, K., & Madden, T. L. (2009). BLAST+: Architecture and applications. *BMC Bioinformatics*, *10*(1), 421. https://doi.org/10.1186/1471-2105-10-421

682 Camargo, A. P., Roux, S., Schulz, F., Babinski, M., Xu, Y., Hu, B., Chain, P. S. G., Nayfach, S., & Kyrpides, N.
683 C. (2023). Identification of mobile genetic elements with geNomad. *Nature Biotechnology*.
684 https://doi.org/10.1038/s41587-023-01953-y
685 Cantalapiedra, C. P., Hernández-Plaza, A., Letunic, I., Bork, P., & Huerta-Cepas, J. (2021). eggNOG-
686 mapper v2: Functional annotation, orthology assignments, and domain prediction at the
687 metagenomic scale. *Molecular Biology and Evolution*, *38*(12), 5825–5829.
688 https://doi.org/10.1093/molbev/msab293
689 Chaumeil, P.-A., Mussig, A. J., Hugenholtz, P., & Parks, D. H. (2020). GTDB-Tk: A toolkit to classify
690 genomes with the Genome Taxonomy Database. *Bioinformatics*, *36*(6), 1925–1927.
691 https://doi.org/10.1093/bioinformatics/btz848
692 Cheng, R., Huang, F., Lu, X., Yan, Y., Yu, B., Wang, X., & Zhu, B. (2023). Prokaryotic Gabija complex senses
693 and executes nucleotide depletion and DNA cleavage for antiviral defense. *Cell Host & Microbe*,
694 *31*(8), 1331-1344.e5. https://doi.org/10.1016/j.chom.2023.06.014
695 Colombi, E., Bertels, F., Doulcier, G., McConnell, E., Pichugina, T., Sohn, K. H., Straub, C., McCann, H. C.,
696 & Rainey, P. B. (2024). Rapid dissemination of host metabolism–manipulating genes via
697 integrative and conjugative elements. *Proceedings of the National Academy of Sciences*, *121*(11),
698 e2309263121. https://doi.org/10.1073/pnas.2309263121
699 Colombi, E., Straub, C., Künzel, S., Templeton, M. D., McCann, H. C., & Rainey, P. B. (2017). Evolution of
700 copper resistance in the kiwifruit pathogen *Pseudomonas syringae* pv. *Actinidiae* through
701 acquisition of integrative conjugative elements and plasmids. *Environmental Microbiology*,
702 *19*(2), 819–832. https://doi.org/10.1111/1462-2920.13662
703 de Sousa, J. A. M., Fillol-Salom, A., Penadés, J. R., & Rocha, E. P. C. (2023). Identification and
704 characterization of thousands of bacteriophage satellites across bacteria. *Nucleic Acids*
705 *Research*, *51*(6), 2759–2777. https://doi.org/10.1093/nar/gkad123

706 Dillingham, M. S., & Kowalczykowski, S. C. (2008). RecBCD enzyme and the repair of double-stranded
707 DNA breaks. *Microbiology and Molecular Biology Reviews*, *72*(4), 642–671.
708 https://doi.org/10.1128/MMBR.00020-08
709 Dmitrijeva, M., Tackmann, J., Matias Rodrigues, J. F., Huerta-Cepas, J., Coelho, L. P., & von Mering, C.
710 (2024). A global survey of prokaryotic genomes reveals the eco-evolutionary pressures driving
711 horizontal gene transfer. *Nature Ecology & Evolution*, *8*(5), 986–998.
712 https://doi.org/10.1038/s41559-024-02357-0
713 Doolittle, W. F. (2024). *Darwinizing Gaia: Natural selection and multispecies community evolution*. The
714 MIT Press.
715 Doolittle, W. F., & Inkpen, S. A. (2018). Processes and patterns of interaction as units of selection: An
716 introduction to ITSNTS thinking. *Proceedings of the National Academy of Sciences*, *115*(16),
717 4006–4014. https://doi.org/10.1073/pnas.1722232115
718 Doron, S., Melamed, S., Ofir, G., Leavitt, A., Lopatina, A., Keren, M., Amitai, G., & Sorek, R. (2018).
719 Systematic discovery of antiphage defense systems in the microbial pangenome. *Science*,
720 *359*(6379), eaar4120. https://doi.org/10.1126/science.aar4120
721 Farr, A. D., Vasileiou, C., Lind, P. A., & Rainey, P. B. (2025). An extreme mutational hotspot in nlpD
722 depends on transcriptional induction of rpoS. *PLOS Genetics*, *21*(1), e1011572.
723 https://doi.org/10.1371/journal.pgen.1011572
724 Faruque, S. M., & Mekalanos, J. J. (2003). Pathogenicity islands and phages in *Vibrio cholerae* evolution.
725 *Trends in Microbiology*, *11*(11), Article 11. https://doi.org/10.1016/j.tim.2003.09.003
726 Faruque, S. M., & Mekalanos, J. J. (2012). Phage-bacterial interactions in the evolution of toxigenic *Vibrio*
727 *cholerae*. *Virulence*, *3*(7), Article 7. https://doi.org/10.4161/viru.22351
728 Faruque, S. M., Zhu, J., Asadulghani, Kamruzzaman, M., & Mekalanos, J. J. (2003). Examination of diverse
729 toxin-coregulated pilus-positive *Vibrio cholerae* strains fails to demonstrate evidence for *Vibrio*

730 pathogenicity island phage. *Infection and Immunity*, *71*(6), 2993–2999.
731 https://doi.org/10.1128/IAI.71.6.2993-2999.2003
732 Fiedoruk, K., Zakrzewska, M., Daniluk, T., Piktel, E., Chmielewska, S., & Bucki, R. (2020). Two lineages of
733 *Pseudomonas aeruginosa* filamentous phages: Structural uniformity over integration
734 preferences. *Genome Biology and Evolution*, *12*(10), 1765–1781.
735 https://doi.org/10.1093/gbe/evaa146
736 Fillol-Salom, A., Bacarizo, J., Alqasmi, M., Ciges-Tomas, J. R., Martínez-Rubio, R., Roszak, A. W., Cogdell,
737 R. J., Chen, J., Marina, A., & Penadés, J. R. (2019). Hijacking the hijackers: *Escherichia coli*
738 pathogenicity islands redirect helper phage packaging for their own benefit. *Molecular Cell*,
739 *75*(5), 1020-1030.e4. https://doi.org/10.1016/j.molcel.2019.06.017
740 Fortmann-Grote, C., Hugoson, E., Summers, J., Theodosiou, L., & Rainey, P. B. (2023). Genome update
741 for *Pseudomonas fluorescens* isolate SBW25. *Microbiology Resource Announcements*, *12*(2),
742 e00637-22. https://doi.org/10.1128/mra.00637-22
743 Frazão, N., Sousa, A., Lässig, M., & Gordo, I. (2019). Horizontal gene transfer overrides mutation in
744 *Escherichia coli* colonizing the mammalian gut. *Proceedings of the National Academy of Sciences*,
745 *116*(36), 17906–17915. https://doi.org/10.1073/pnas.1906958116
746 Griffith, F. (1928). The significance of pneumococcal types. *Journal of Hygiene*, *27*(2), 113–159.
747 https://doi.org/10.1017/S0022172400031879
748 Grindley, N. D. F., Whiteson, K. L., & Rice, P. A. (2006). Mechanisms of site-specific recombination.
749 *Annual Review of Biochemistry*, *75*(1), 567–605.
750 https://doi.org/10.1146/annurev.biochem.73.011303.073908
751 Groth, A. C., & Calos, M. P. (2004). Phage integrases: Biology and applications. *Journal of Molecular*
752 *Biology*, *335*(3), 667–678. https://doi.org/10.1016/j.jmb.2003.09.082

753 Groussin, M., Poyet, M., Sistiaga, A., Kearney, S. M., Moniz, K., Noel, M., Hooker, J., Gibbons, S. M.,
754 Segurel, L., Froment, A., Mohamed, R. S., Fezeu, A., Juimo, V. A., Lafosse, S., Tabe, F. E., Girard,
755 C., Iqaluk, D., Nguyen, L. T. T., Shapiro, B. J., … Alm, E. J. (2021). Elevated rates of horizontal gene
756 transfer in the industrialized human microbiome. *Cell*, *184*(8), 2053-2067.e18.
757 https://doi.org/10.1016/j.cell.2021.02.052
758 Guo, L., Sattler, L., Shafqat, S., Graumann, P. L., & Bramkamp, M. (2022). A bacterial dynamin-like
759 protein confers a novel phage resistance strategy on the population level in *Bacillus subtilis*.
760 *MBio*, *13*(1). https://journals.asm.org/doi/10.1128/mbio.03753-21
761 Hackl, T., Laurenceau, R., Ankenbrand, M. J., Bliem, C., Cariani, Z., Thomas, E., Dooley, K. D., Arellano, A.
762 A., Hogle, S. L., Berube, P., Leventhal, G. E., Luo, E., Eppley, J. M., Zayed, A. A., Beaulaurier, J.,
763 Stepanauskas, R., Sullivan, M. B., DeLong, E. F., Biller, S. J., & Chisholm, S. W. (2023). Novel
764 integrative elements and genomic plasticity in ocean ecosystems. *Cell*, *186*(1), 47-62.e16.
765 https://doi.org/10.1016/j.cell.2022.12.006
766 Hall, J. P. J., Wood, A. J., Harrison, E., & Brockhurst, M. A. (2016). Source–sink plasmid transfer dynamics
767 maintain gene mobility in soil bacterial communities. *Proceedings of the National Academy of*
768 *Sciences*, *113*(29), 8260–8265. https://doi.org/10.1073/pnas.1600974113
769 Hmelo, L. R., Borlee, B. R., Almblad, H., Love, M. E., Randall, T. E., Tseng, B. S., Lin, C., Irie, Y., Storek, K.
770 M., Yang, J. J., Siehnel, R. J., Howell, P. L., Singh, P. K., Tolker-Nielsen, T., Parsek, M. R.,
771 Schweizer, H. P., & Harrison, J. J. (2015). Precision-engineering the *Pseudomonas aeruginosa*
772 genome with two-step allelic exchange. *Nature Protocols*, *10*(11), 1820–1841.
773 https://doi.org/10.1038/nprot.2015.115
774 Hussain, F. A., Dubert, J., Elsherbini, J., Murphy, M., VanInsberghe, D., Arevalo, P., Kauffman, K., Rodino-
775 Janeiro, B. K., Gavin, H., Gomez, A., Lopatina, A., Le Roux, F., & Polz, M. F. (2021). Rapid

776 evolutionary turnover of mobile genetic elements drives bacterial resistance to phages. *Science*,
777 *374*(6566), 488–492. https://doi.org/10.1126/science.abb1083
778 Hyatt, D., Chen, G.-L., LoCascio, P. F., Land, M. L., Larimer, F. W., & Hauser, L. J. (2010). Prodigal:
779 Prokaryotic gene recognition and translation initiation site identification. *BMC Bioinformatics*,
780 *11*(1), 119. https://doi.org/10.1186/1471-2105-11-119
781 Ibarra-Chávez, R., Hansen, M. F., Pinilla-Redondo, R., Seed, K. D., & Trivedi, U. (2021). Phage satellites
782 and their emerging applications in biotechnology. *FEMS Microbiology Reviews*, *45*(6), fuab031.
783 https://doi.org/10.1093/femsre/fuab031
784 Ishikawa, T., Watabe, K., Mukohara, Y., & Nakamura, H. (1997). Mechanism of stereospecific conversion
785 of DL-5-substituted hydantoins to the corresponding L-amino acids by *Pseudomonas* sp. Strain
786 NS671. *Bioscience, Biotechnology, and Biochemistry*, *61*(1), 185–187.
787 https://doi.org/10.1271/bbb.61.185
788 Johnson, M. C., Laderman, E., Huiting, E., Zhang, C., Davidson, A., & Bondy-Denomy, J. (2023). Core
789 defense hotspots within *Pseudomonas aeruginosa* are a consistent and rich source of anti-phage
790 defense systems. *Nucleic Acids Research*, *51*(10), 4995–5005.
791 https://doi.org/10.1093/nar/gkad317
792 Jones, P., Binns, D., Chang, H.-Y., Fraser, M., Li, W., McAnulla, C., McWilliam, H., Maslen, J., Mitchell, A.,
793 Nuka, G., Pesseat, S., Quinn, A. F., Sangrador-Vegas, A., Scheremetjew, M., Yong, S.-Y., Lopez, R.,
794 & Hunter, S. (2014). InterProScan 5: Genome-scale protein function classification.
795 *Bioinformatics*, *30*(9), 1236–1240. https://doi.org/10.1093/bioinformatics/btu031
796 Karaolis, D. K. R., Somara, S., Maneval, D. R., Johnson, J. A., & Kaper, J. B. (1999). A bacteriophage
797 encoding a pathogenicity island, a type-IV pilus and a phage receptor in cholera bacteria.
798 *Nature*, *399*(6734), Article 6734. https://doi.org/10.1038/20715

Koutsovoulos, G. D., Granjeon Noriot, S., Bailly-Bechet, M., Danchin, E. G. J., & Rancurel, C. (2022). AvP: A software package for automatic phylogenetic detection of candidate horizontal gene transfers. *PLOS Computational Biology*, *18*(11), e1010686. https://doi.org/10.1371/journal.pcbi.1010686

Lang, A. S., Zhaxybayeva, O., & Beatty, J. T. (2012). Gene transfer agents: Phage-like elements of genetic exchange. *Nature Reviews Microbiology*, *10*(7), 472–482. https://doi.org/10.1038/nrmicro2802

Laughlin, T. G., Deep, A., Prichard, A. M., Seitz, C., Gu, Y., Enustun, E., Suslov, S., Khanna, K., Birkholz, E. A., Armbruster, E., McCammon, J. A., Amaro, R. E., Pogliano, J., Corbett, K. D., & Villa, E. (2022). Architecture and self-assembly of the jumbo bacteriophage nuclear shell. *Nature*, *608*(7922), 429–435. https://doi.org/10.1038/s41586-022-05013-4

Lederberg, J., & Tatum, E. L. (1946). Gene recombination in *Escherichia coli*. *Nature*, *158*(4016), 558–558. https://doi.org/10.1038/158558b0

Lenski, R. E. (2017). Experimental evolution and the dynamics of adaptation and genome evolution in microbial populations. *The ISME Journal*, *11*(10), 2181–2194. https://doi.org/10.1038/ismej.2017.69

Lenski, R. E., Rose, M. R., Simpson, S. C., & Tadler, S. C. (1991). Long-term experimental evolution in *Escherichia coli*. I. Adaptation and divergence during 2,000 generations. *The American Naturalist*, *138*(6), 1315–1341. https://doi.org/10.1086/285289

Lenton, T. M., Kohler, T. A., Marquet, P. A., Boyle, R. A., Crucifix, M., Wilkinson, D. M., & Scheffer, M. (2021). Survival of the systems. *Trends in Ecology & Evolution*, *36*(4), 333–344. https://doi.org/10.1016/j.tree.2020.12.003

Li, D., Liu, C.-M., Luo, R., Sadakane, K., & Lam, T.-W. (2015). MEGAHIT: An ultra-fast single-node solution for large and complex metagenomics assembly via succinct *de Bruijn* graph. *Bioinformatics*, *31*(10), 1674–1676. https://doi.org/10.1093/bioinformatics/btv033

823 Lilley, A. K., & Bailey, M. J. (1997a). Impact of plasmid pQBR103 acquisition and carriage on the
824 phytosphere fitness of *Pseudomonas fluorescens* SBW25: Burden and benefit. *Applied and*
825 *Environmental Microbiology*, *63*(4), 1584–1587. https://doi.org/10.1128/aem.63.4.1584-
826 1587.1997
827 Lilley, A. K., & Bailey, M. J. (1997b). The acquisition of indigenous plasmids by a genetically marked
828 pseudomonad population colonizing the sugar beet phytosphere is related to local
829 environmental conditions. *Applied and Environmental Microbiology*, *63*(4), 1577–1583.
830 https://doi.org/10.1128/aem.63.4.1577-1583.1997
831 Lindsay, J. A., Ruzin, A., Ross, H. F., Kurepina, N., & Novick, R. P. (1998). The gene for toxic shock toxin is
832 carried by a family of mobile pathogenicity islands in *Staphylococcus aureus*. *Molecular*
833 *Microbiology*, *29*(2), 527–543. https://doi.org/10.1046/j.1365-2958.1998.00947.x
834 Low, S. J., Džunková, M., Chaumeil, P.-A., Parks, D. H., & Hugenholtz, P. (2019). Evaluation of a
835 concatenated protein phylogeny for classification of tailed double-stranded DNA viruses
836 belonging to the order Caudovirales. *Nature Microbiology*, *4*(8), 1306–1315.
837 https://doi.org/10.1038/s41564-019-0448-z
838 Marrs, B. (1974). Genetic recombination in *Rhodopseudomonas capsulata*. *Proceedings of the National*
839 *Academy of Sciences*, *71*(3), 971–973. https://doi.org/10.1073/pnas.71.3.971
840 Meier-Kolthoff, J. P., & Göker, M. (2017). VICTOR: Genome-based phylogeny and classification of
841 prokaryotic viruses. *Bioinformatics*, *33*(21), 3396–3404.
842 https://doi.org/10.1093/bioinformatics/btx440
843 Nayfach, S., Páez-Espino, D., Call, L., Low, S. J., Sberro, H., Ivanova, N. N., Proal, A. D., Fischbach, M. A.,
844 Bhatt, A. S., Hugenholtz, P., & Kyrpides, N. C. (2021). Metagenomic compendium of 189,680
845 DNA viruses from the human gut microbiome. *Nature Microbiology*, *6*(7), 960–970.
846 https://doi.org/10.1038/s41564-021-00928-6

Néron, B., Denise, R., Coluzzi, C., Touchon, M., Rocha, E. P. C., & Abby, S. S. (2023). MacSyFinder v2: Improved modelling and search engine to identify molecular systems in genomes. *Peer Community Journal*, *3*, e28. https://doi.org/10.24072/pcjournal.250

Novick, R. P., Christie, G. E., & Penadés, J. R. (2010). The phage-related chromosomal islands of Gram-positive bacteria. *Nature Reviews Microbiology*, *8*(8), 541–551. https://doi.org/10.1038/nrmicro2393

Ofir, G., Melamed, S., Sberro, H., Mukamel, Z., Silverman, S., Yaakov, G., Doron, S., & Sorek, R. (2017). DISARM is a widespread bacterial defence system with broad anti-phage activities. *Nature Microbiology*, *3*(1), 90–98. https://doi.org/10.1038/s41564-017-0051-0

O'Shea, Y. A., & Boyd, E. F. (2002). Mobilization of the *Vibrio* pathogenicity island between *Vibrio cholerae* isolates mediated by CP-T1 generalized transduction. *FEMS Microbiology Letters*, *214*(2), 153–157. https://doi.org/10.1111/j.1574-6968.2002.tb11339.x

Penadés, J. R., Seed, K. D., Chen, J., Bikard, D., & Rocha, E. P. C. (2025). Genetics, ecology and evolution of phage satellites. *Nature Reviews Microbiology*. https://doi.org/10.1038/s41579-025-01156-z

Quistad, S. D., Doulcier, G., & Rainey, P. B. (2020). Experimental manipulation of selfish genetic elements links genes to microbial community function. *Philosophical Transactions of the Royal Society B: Biological Sciences*, *375*, 20190681. https://doi.org/10.1098/rstb.2019.0681

Rainey, P. B., & Quistad, S. D. (2020). Toward a dynamical understanding of microbial communities. *Philosophical Transactions of the Royal Society B: Biological Sciences*, *375*, 20190248. https://doi.org/10.1098/rstb.2019.0248

Rainey, P. B., Remigi, P., Farr, A. D., & Lind, P. A. (2017). Darwin was right: Where now for experimental evolution? *Current Opinion in Genetics & Development*, *47*, 102–109. https://doi.org/10.1016/j.gde.2017.09.003

870 Rainey, P. B., & Travisano, M. (1998). Adaptive radiation in a heterogeneous environment. *Nature*,
871 *394*(6688), 69–72. https://doi.org/10.1038/27900
872 Roughgarden, J. (2020). Holobiont evolution: Mathematical model with vertical vs. horizontal
873 microbiome transmission. *Philosophy, Theory, and Practice in Biology*, *12*(20220112).
874 https://doi.org/10.3998/ptpbio.16039257.0012.002
875 Rousset, F., Depardieu, F., Miele, S., Dowding, J., Laval, A.-L., Lieberman, E., Garry, D., Rocha, E. P. C.,
876 Bernheim, A., & Bikard, D. (2022). Phages and their satellites encode hotspots of antiviral
877 systems. *Cell Host & Microbe*, *30*(5), 740-753.e5. https://doi.org/10.1016/j.chom.2022.02.018
878 Schlechter, R. O., Jun, H., Bernach, M., Oso, S., Boyd, E., Muñoz-Lintz, D. A., Dobson, R. C. J., Remus, D.
879 M., & Remus-Emsermann, M. N. P. (2018). Chromatic bacteria – A broad host-range plasmid and
880 chromosomal insertion toolbox for fluorescent protein expression in bacteria. *Frontiers in*
881 *Microbiology*, *9*, 3052. https://doi.org/10.3389/fmicb.2018.03052
882 Seemann, T. (2014). Prokka: Rapid prokaryotic genome annotation. *Bioinformatics*, *30*(14), 2068–2069.
883 https://doi.org/10.1093/bioinformatics/btu153
884 Sievers, F., Wilm, A., Dineen, D., Gibson, T. J., Karplus, K., Li, W., Lopez, R., McWilliam, H., Remmert, M.,
885 Söding, J., Thompson, J. D., & Higgins, D. G. (2011). Fast, scalable generation of high-quality
886 protein multiple sequence alignments using Clustal Omega. *Molecular Systems Biology*, *7*(539),
887 1–6. https://doi.org/10.1038/msb.2011.75
888 Silby, M. W., Cerdeño-Tárraga, A. M., Vernikos, G. S., Giddens, S. R., Jackson, R. W., Preston, G. M.,
889 Zhang, X.-X., Moon, C. D., Gehrig, S. M., Godfrey, S. A., Knight, C. G., Malone, J. G., Robinson, Z.,
890 Spiers, A. J., Harris, S., Challis, G. L., Yaxley, A. M., Harris, D., Seeger, K., … Thomson, N. R. (2009).
891 Genomic and genetic analyses of diversity and plant interactions of *Pseudomonas fluorescens*.
892 *Genome Biology*, *10*(5), R51. https://doi.org/10.1186/gb-2009-10-5-r51

Sullivan, J. T., & Ronson, C. W. (1998). Evolution of rhizobia by acquisition of a 500-kb symbiosis island that integrates into a phe-tRNA gene. *Proceedings of the National Academy of Sciences*, *95*(9), 5145–5149. https://doi.org/10.1073/pnas.95.9.5145

Sullivan, M. J., Petty, N. K., & Beatson, S. A. (2011). Easyfig: A genome comparison visualizer. *Bioinformatics*, *27*(7), 1009–1010. https://doi.org/10.1093/bioinformatics/btr039

Tatusov, R. L. (2000). The COG database: A tool for genome-scale analysis of protein functions and evolution. *Nucleic Acids Research*, *28*(1), 33–36. https://doi.org/10.1093/nar/28.1.33

Tesson, F., Hervé, A., Mordret, E., Touchon, M., d'Humières, C., Cury, J., & Bernheim, A. (2022). Systematic and quantitative view of the antiviral arsenal of prokaryotes. *Nature Communications*, *13*(1), 2561. https://doi.org/10.1038/s41467-022-30269-9

Tock, M. R., & Dryden, D. T. (2005). The biology of restriction and anti-restriction. *Current Opinion in Microbiology*, *8*(4), 466–472. https://doi.org/10.1016/j.mib.2005.06.003

van Dijk, B., Buffard, P., Farr, A. D., Giersdorf, F., Meijer, J., Dutilh, B. E., & Rainey, P. B. (2023). Identifying and tracking mobile elements in evolving compost communities yields insights into the nanobiome. *ISME Communications*, *3*(90). https://doi.org/10.1101/2023.02.02.526783

Wang, M., Liu, G., Liu, M., Tai, C., Deng, Z., Song, J., & Ou, H.-Y. (2024). ICEberg 3.0: Functional categorization and analysis of the integrative and conjugative elements in bacteria. *Nucleic Acids Research*, *52*, D732–D737. https://doi.org/10.1093/nar/gkad935

Wang, X., Kim, Y., & Wood, T. K. (2009). Control and benefits of CP4-57 prophage excision in *Escherichia coli* biofilms. *The ISME Journal*, *3*(10), 1164–1179. https://doi.org/10.1038/ismej.2009.59

Woods, L. C., Gorrell, R. J., Taylor, F., Connallon, T., Kwok, T., & McDonald, M. J. (2020). Horizontal gene transfer potentiates adaptation by reducing selective constraints on the spread of genetic variation. *Proceedings of the National Academy of Sciences*, *117*(43), 26868–26875. https://doi.org/10.1073/pnas.2005331117

917 Xie, Z., & Tang, H. (2017). ISEScan: Automated identification of insertion sequence elements in
918 prokaryotic genomes. *Bioinformatics*, *33*(21), 3340–3347.
919 https://doi.org/10.1093/bioinformatics/btx433
920 Yuan, L., Lu, H., Li, F., Nielsen, J., & Kerkhoven, E. J. (2023). HGTphyloDetect: Facilitating the
921 identification and phylogenetic analysis of horizontal gene transfer. *Briefings in Bioinformatics*,
922 *24*(2), bbad035. https://doi.org/10.1093/bib/bbad035
923 Zinder, N. D., & Lederberg, J. (1952). Genetic exchange in *Salmonella*. *Journal of Bacteriology*, *64*(5),
924 679–699. https://doi.org/10.1128/jb.64.5.679-699.1952
925
926

927 ## Figures

928

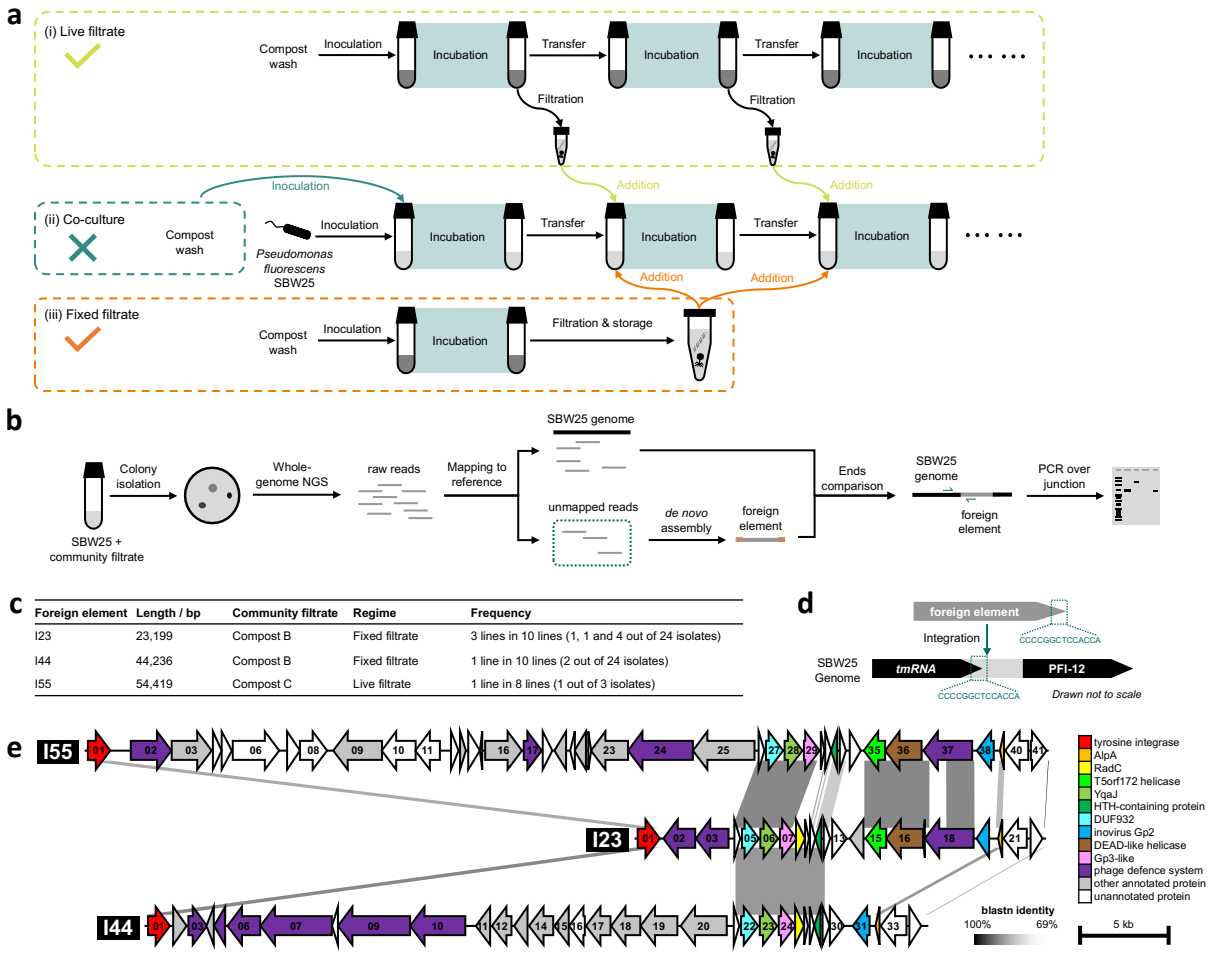

Foreign element	Length / bp	Community filtrate	Regime	Frequency
I23	23,199	Compost B	Fixed filtrate	3 lines in 10 lines (1, 1 and 4 out of 24 isolates)
I44	44,236	Compost B	Fixed filtrate	1 line in 10 lines (2 out of 24 isolates)
I55	54,419	Compost C	Live filtrate	1 line in 8 lines (1 out of 3 isolates)

929

930

931 **Fig. 1**. Experimental evolution and detection of foreign elements

932 **a**. Three serial-propagation regimes to evolve SBW25 populations. (i) live filtrate regime; (ii) co-culture
933 regime; (iii) fixed filtrate regime. Components within each box are specific to each regime, and
934 components outside of boxes are common to all regimes.

935 **b**. The pipeline for screening and confirming SBW25 strains carrying foreign elements inserted into the
936 genome.

937 **c**. Basic information for the 3 foreign elements detected. The table lists the number of base pairs of each
938 foreign element, the name of the compost community from which the community filtrate was
939 generated, the serial-propagation regime, the number of parallel lines from which isolates with the
940 foreign element were detected, and the number of isolates containing the foreign element in each such
941 line.

942 **d**. Insertion site of the foreign elements in the SBW25 genome. Upon insertion, two 14 bp direct repeats
943 flank the foreign element. The direct repeats at the 5'-end and 3'-end of the element were treated as

944 from SBW25 genome and from the foreign element, respectively, despite the exact origin of each repeat
945 is unknown.

946 **e**. The aligned genetic maps of the 3 foreign elements, I23, I44 and I55. The alignment was created by
947 Easyfig (M. J. Sullivan et al., 2011). Parallelograms between MGEs indicate similar genomic regions based
948 on blastn. The ORFs were numbered serially from 5-end to 3'-end for each MGE, and colored according
949 to annotations. Detailed annotations of each ORF are listed in Table S4.

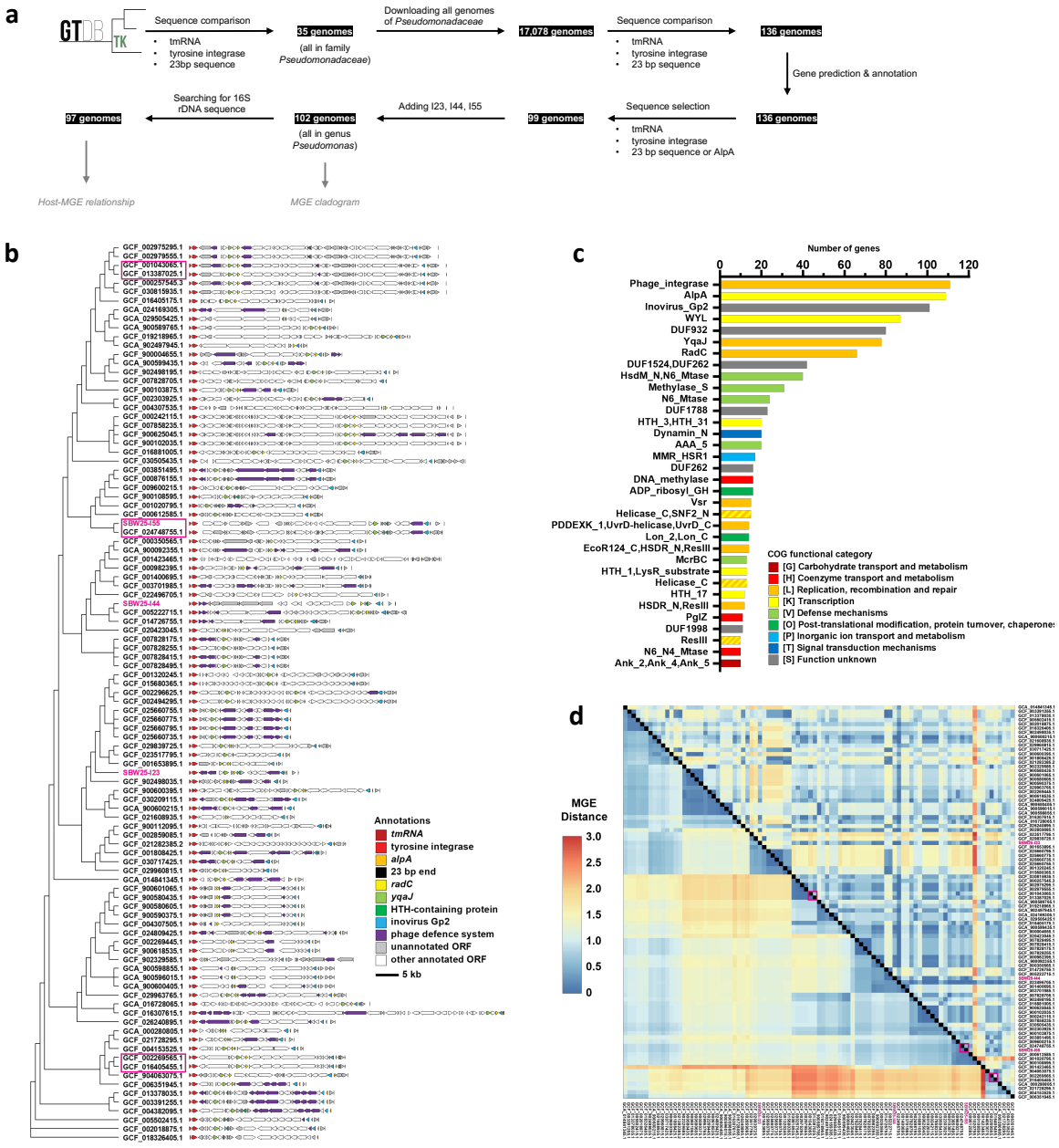

Fig. 2. Bioinformatic analysis of similar elements

a. Bioinformatic pipeline for detection of similar elements to I55. Bullet points below "sequence comparison" and "sequence selection" represent the criteria for comparison and searching, respectively.

b. Cladogram and genomic representations of I23, I44, I55 and similar MGEs (identified by NCBI RefSeq assembly indices). Basis for construction of the tree is summarized in the text. Shape of the tree represents inferred evolutionary relationship but not evolutionary distances.

959 **c**. Rank abundance of annotated genes of different functional classes in panel b. Genes occurring at least
960 10 times are illustrated. A full rank abundance table is in Table S6. Colors represent COG functional
961 categories.

962 **d**. Pairwise distances between the MGEs (shown in lower-left), and pairwise distances between their
963 corresponding hosts (shown in upper-right). MGEs and hosts are identified by NCBI RefSeq assembly
964 indices. Basis for construction and interpretation of the heatmap is summarized in the text. Pink boxes
965 highlight pairs of strains with almost identical MGE, but remarkably different 16S sequence. Annotations
966 of those MGEs are boxed in pink in panel b.

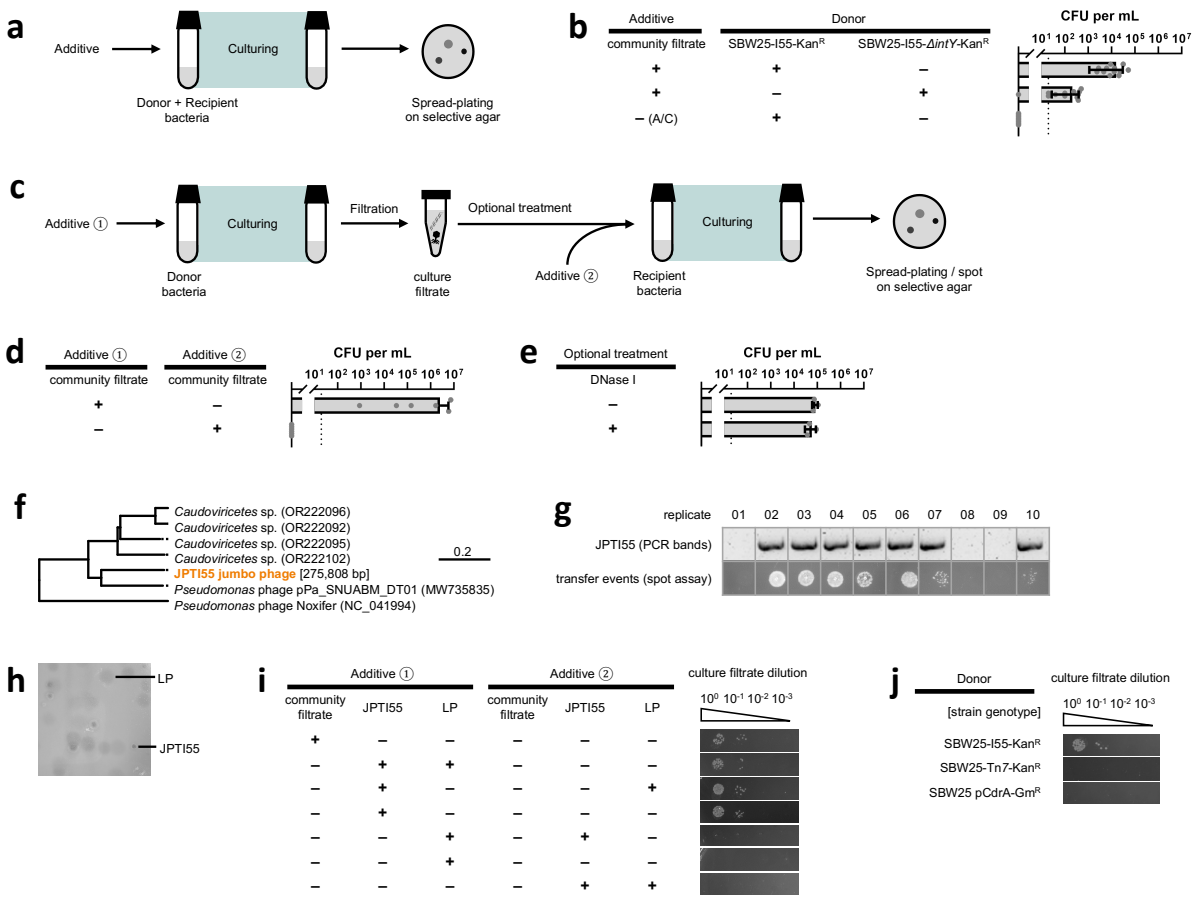

Fig. 3. Intercellular transfer of I55

a. Schematic of the one-step intercellular transfer assay.

b. The densities of CFUs on selective agar in the one-step intercellular transfer assay, to test whether and in which environment the I55 can transfer intercellularly. For all treatments, the recipient was SBW25-Tet^R, and the final culture was spread plated on agar with Kan + Tet. Data are mean ± s.d. The dotted line represents the detection limit of the assay. The label A/C represents autoclaved filtrate. For each treatment, 8 to 12 biological replicates were used. Mann-Whitney test was applied to test the effect of IntA ($p < 0.0001$) when the community filtrate was added.

c. Schematic of the two-step intercellular transfer assay.

d. The densities of CFUs on selective agar in the two-step intercellular transfer assay, to test whether I55 transfers intercellular via cell-to-cell conjugation. For all treatments, the donor was SBW25-I55-Kan^R, the recipient was SBW25-Tet^R, no optional treatment of culture filtrate was conducted, and the final culture was spread plated on agar with Kan + Tet. Data are mean ± s.d. The dotted line represents the detection limit of the assay. For each treatment, 8 biological replicates were used.

e. The densities of CFUs on selective agar in the two-step intercellular transfer assay, to test whether I55 transfers intercellular via transformation of naked DNA. The DNase I was confirmed to be active in

985 digesting circular and linear DNA in the environment of community filtrate (see Fig. E3). For all
986 treatments, the donor was SBW25-I55-Kan^R, the recipient was SBW25-Tet^R, additive ① was community
987 filtrate, additive ② was none, and the final culture was spread plated on agar with Kan + Tet. Data are
988 mean ± s.d. The dotted line represents the detection limit of the assay. For each treatment, 3 biological
989 replicates were used. Mann-Whitney test was applied to test the effect of DNase I (p = 0.4000) in
990 transfer.

991 **f**. A phylogeny of relatives of the jumbo bacteriophage JPTI55. The complete genome of JPTI55 was *de*
992 *novo* assembled from metagenomic sequencing, later corrected by whole genome sequencing of phage
993 isolates. The genome of JPTI55 is circular and 275,808 bp in length. Distance on the phylogeny
994 represents identity in nucleotide sequences.

995 **g**. The relationship between the presence of JPTI55 and the presence of transfer events. Two-step
996 intercellular transfer assay was conducted. For all treatments, the donor was SBW25-I55-Kan^R, the
997 recipient was SBW25-Tet^R, additive ① was a certain dilution level of community filtrate, additive ②
998 was none, no optional treatment of culture filtrate was conducted, and the final cultures were
999 independently spotted on agar with Kan + Tet. There were 10 technical replicates for each type of
1000 additive ①. In addition, the final cultures were filtrated and tested for the presence of JPTI55 by PCR.
1001 Picture here corresponds to the set of 10 replicates receiving a certain dilution level of community
1002 filtrate as additive ①, at which around half of the replicates contained JPTI55 and the other half did
1003 not. Photos of five additional sets of replicates, receiving community filtrate from another dilution level
1004 or from another biological replicate of community filtrate, can be found in Fig. S1.

1005 **h**. Typical photos of the plaque assay of the community filtrate against SBW25 wild type as hosts, using
1006 0.2% top agar in M9+Glucose medium. Picture contrast was altered to facilitate visualization of the
1007 plaques. The identities of the plaques were confirmed by PCR.

1008 **i**. The presence or absence of transfer events along a dilution series of culture filtrate in the two-step
1009 intercellular transfer assay, to test the transfer ability of the UFV-like bacteriophage and the JPTI55
1010 jumbo bacteriophage. For all treatments, the donor was SBW25-I55-Kan^R, the recipient was SBW25-Tet^R,
1011 at the optional treatment step the culture filtrate was diluted along a dilution series and each dilution
1012 was separately added to independent recipient cultures, and the final cultures were independently
1013 spotted on agar with Kan + Tet. Picture contrast was altered to facilitate visualization of the spots.
1014 Photos of two additional biological replicates can be found in Fig. S2.

1015 **j**. The presence or absence of transfer events along a dilution series of culture filtrate in the two-step
1016 intercellular transfer assay, to test whether JPTI55 could mobilize chromosomal markers or plasmids.
1017 For all treatments, the recipient was SBW25-Tet^R, additive ① was JPTI55, additive ② was none, at the
1018 optional treatment step the culture filtrate was diluted along a dilution series and each dilution was
1019 separately added to independent recipient cultures, and the final cultures were independently spotted
1020 on agar with Kan + Tet (except for the treatment with donor strain SBW25 pCdrA-Gm^R, which was
1021 spotted on agar with Gm + Tet). Picture contrast was altered to facilitate visualization of the spots.
1022 Photos of two additional biological replicates can be found in Fig. S3.

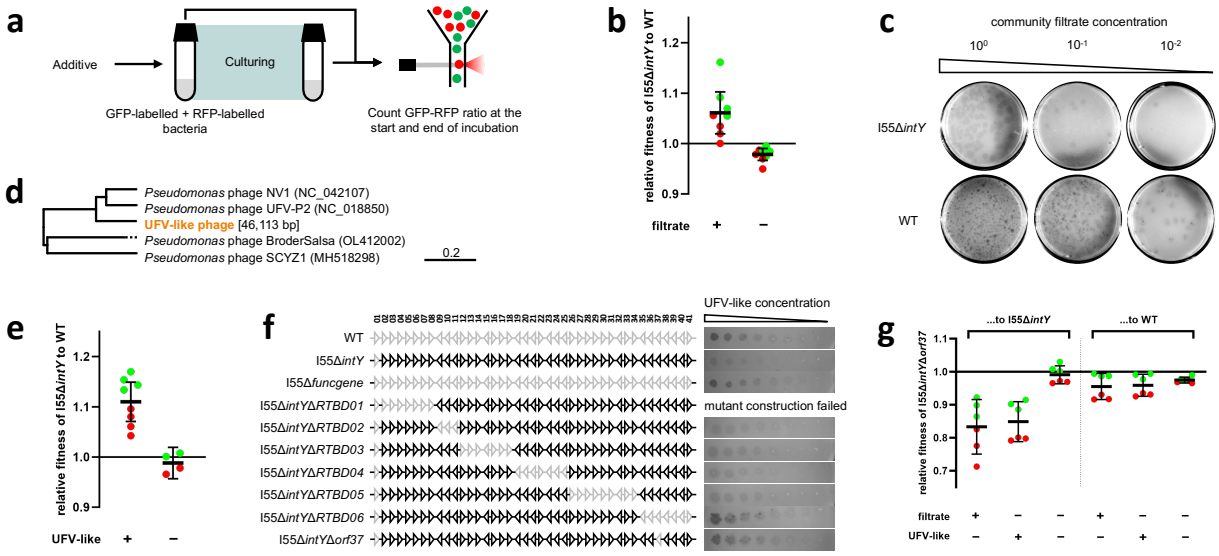

Fig. 4. Fitness advantage and phage defense activity of I55

a. Schematic of fluorescent fitness assay. To eliminate the possibility for I55 to transfer among cells during the fitness assay, all strains carrying I55 had *intY* deleted, because SBW25-I55Δ*intY* was previously shown to be incapable of excision from the genome (see Fig. E2). Moreover, to ensure the two competing strains have identical genetic backgrounds, ancestral SBW25 was re-constructed by deleting I55 from SBW25-I55Δ*intY*.

b. Fluorescent fitness assay results for SBW25-I55Δ*intY* (strain MPB39132/MPB39136) relative to wild type (strain MPB39379/MPB39459), in presence or absence of community filtrate. Data are mean ± 95% CI. In the Filtrate + and - treatments, stored filtrate aliquots from compost C and from SBW25 were added, respectively. The color of each data point corresponds to the color of the fluorescent marker added to SBW25-I55Δ*intY*. For each treatment, 8 biological replicates (4 for either tagging strategy) were used. One sample *t*-tests were applied to test the relative fitness values against 1 when the community filtrate was added ($p = 0.0104$) and not added ($p = 0.0033$).

c. Typical photos of the plaque assay of the community filtrate against SBW25-I55Δ*intY* or wild type as hosts. Picture contrast was altered to facilitate visualization of the plaques. Photos of three additional biological replicates can be found in Fig. S4.

d. A phylogeny of relatives of the UFV-like bacteriophage. The complete genome of the UFV-like phage was *de novo* assembled from whole genome sequences. The genome of UFV-like phage is circular and 46,113 bp in length. Distance on the phylogeny represents identity in nucleotide sequences.

e. Fluorescent fitness assay results for SBW25-I55Δ*intY* relative to wild type, in presence or absence of the UFV-like bacteriophage. Data are mean ± 95% CI. The color of each data point corresponds to the color of the fluorescent marker added to SBW25-I55ΔintY. For each treatment, 8 or 4 biological replicates (4 or 2 for either tagging strategy, respectively) were used. One sample *t*-tests were applied to test the relative fitness values against 1 when the UFV-like bacteriophage was added ($p = 0.0003$) and not added ($p = 0.3118$).

1050 **f.** Systematic deletion assay and phage spot assay to identify the phage defense gene. Regions of I55
1051 deleted are shown in grey. Picture contrast was altered to facilitate visualization of the spots. Photos of
1052 two additional biological replicates can be found in Fig. S5.

1053 **g**. Fluorescent fitness assay results for SBW25-I55Δ*intY*Δ*orf37* (strain MPB42855) relative to SBW25-
1054 I55Δ*intY* or wild type, in presence or absence of the community filtrate or UFV-like bacteriophage. Data
1055 are mean ± 95% CI. The color of each data point corresponds to the color of the fluorescent marker
1056 added to for SBW25-I55Δ*intY*Δ*orf37*. For each treatment, 6 biological replicates (3 for either tagging
1057 strategy, respectively) were used. One sample *t*-tests were applied to test the relative fitness values of
1058 SBW25-I55Δ*intY*Δ*orf37* relative to SBW25-I55Δ*intY* against 1 when the community filtrate was added (p
1059 = 0.0035), when the UFV-like bacteriophage was added (p = 0.0014), and when there was no additive (p
1060 = 0.4237). The same tests were applied to test the relative fitness values of SBW25-I55Δ*intY*Δ*orf37*
1061 relative to wild type against 1 when the community filtrate was added (p = 0.0331), when the UFV-like
1062 bacteriophage was added (p = 0.0252), and when there was no additive (p = 0.0008).